



# **JGR** Atmospheres

## ب

### RESEARCH ARTICLE

10.1029/2023JD040142

#### **Key Points:**

- New analyses of Greenland ice-core records of volcanism between 936 and 943 CE
- Icelandic eruptions from Grímsvötn and Bárðarbunga-Veiðivötn detected between 936 and 941 CE, and major Eldgjá emission in 939–940 CE
- Various silicic eruptions identified, including the Jala Pumice (Mexico), providing new and valuable transcontinental tephra isochrons

#### **Supporting Information:**

Supporting Information may be found in the online version of this article.

#### Correspondence to:

W. Hutchison, wh39@st-andrews.ac.uk

#### Citation:

Hutchison, W., Gabriel, I., Plunkett, G., Burke, A., Sugden, P., Innes, H., et al. (2024). High-resolution ice-core analyses identify the Eldgjá eruption and a cluster of Icelandic and trans-continental tephras between 936 and 943 CE. *Journal of Geophysical Research: Atmospheres*, 129, e2023JD040142. https://doi.org/10.1029/2023JD040142

Received 5 OCT 2023 Accepted 5 AUG 2024

© 2024. The Author(s). This is an open access article under the terms of the Creative Commons Attribution License, which permits use, distribution and reproduction in any medium, provided the original work is properly cited.

### High-Resolution Ice-Core Analyses Identify the Eldgjá Eruption and a Cluster of Icelandic and Trans-Continental Tephras Between 936 and 943 CE

William Hutchison<sup>1</sup>, Imogen Gabriel<sup>2</sup>, Gill Plunkett<sup>3</sup>, Andrea Burke<sup>1</sup>, Patrick Sugden<sup>1</sup>, Helen Innes<sup>1</sup>, Siwan Davies<sup>4</sup>, William M. Moreland<sup>5</sup>, Kirstin Krüger<sup>6</sup>, Rob Wilson<sup>1</sup>, Bo M. Vinther<sup>7</sup>, Dorthe Dahl-Jensen<sup>7</sup>, Johannes Freitag<sup>8</sup>, Clive Oppenheimer<sup>9,10</sup>, Nathan J. Chellman<sup>11</sup>, Michael Sigl<sup>2</sup>, and Joseph R. McConnell<sup>11</sup>

<sup>1</sup>School of Earth and Environmental Sciences, University of St Andrews, St Andrews, UK, <sup>2</sup>Climate and Environmental Physics & Oeschger Centre for Climate Change Research, University of Bern, Bern, Switzerland, <sup>3</sup>Archaeology & Palaeoecology, School of Natural and Built Environment, Queen's University Belfast, Belfast, UK, <sup>4</sup>Department of Geography, College of Science, Swansea University, Swansea, UK, <sup>5</sup>Institute of Earth Sciences, University of Iceland, Reykjavík, Iceland, <sup>6</sup>Department of Geosciences, University of Oslo, Oslo, Norway, <sup>7</sup>Section for the Physics of Ice, Climate, and Earth, Centre for Ice and Climate, Niels Bohr Institute, University of Copenhagen, Copenhagen, Denmark, <sup>8</sup>Alfred Wegener Institute, Helmholtz Centre for Polar and Marine Research, Bremerhaven, Germany, <sup>9</sup>Department of Geography, University of Cambridge, Cambridge, UK, <sup>10</sup>Istituto Nazionale di Geofisica e Vulcanologia, Osservatorio Etneo, Catania, Italy, <sup>11</sup>Division of Hydrologic Sciences, Desert Research Institute, Reno, NV, USA

**Abstract** The Eldgjá eruption is the largest basalt lava flood of the Common Era. It has been linked to a major ice-core sulfur (S) spike in 939-940 CE and Northern Hemisphere summer cooling in 940 CE. Despite its magnitude and potential climate impacts, uncertainties remain concerning the eruption timeline, atmospheric dispersal of emitted volatiles, and coincident volcanism in Iceland and elsewhere. Here, we present a comprehensive analysis of Greenland ice-cores from 936 to 943 CE, revealing a complex volatile record and cryptotephra with numerous geochemical populations. Transitional alkali basalt tephra matching Eldgjá are found in 939-940 CE, while tholeiitic basalt shards present in 936/937 CE and 940/941 CE are compatible with contemporaneous Icelandic eruptions from Grímsvötn and Bárðarbunga-Veiðivötn systems (including V-Sv tephra). We also find four silicic tephra populations, one of which we link to the Jala Pumice of Ceboruco (Mexico) at 941  $\pm$  1 CE. Triple S isotopes,  $\Delta^{33}$ S, spanning 936–940 CE are indicative of upper tropospheric/ lower stratospheric transport of aerosol sourced from the Icelandic fissure eruptions. However, anomalous  $\Delta^{33}$ S (down to -0.4%) in 940–941 CE evidence stratospheric aerosol transport consistent with summer surface cooling revealed by tree-ring reconstructions. Tephra associated with the anomalous  $\Delta^{33}$ S have a variety of compositions, complicating the attribution of climate cooling to Eldgiá alone. Nevertheless, our study confirms a major S emission from Eldgjá in 939-940 CE and implicates Eldgjá and a cluster of eruptions as triggers of summer cooling, severe winters, and privations in ~940 CE.

Plain Language Summary The eruption of Eldgjá in the tenth century is the largest lava flood in the history of Iceland. Although Eldgjá emitted immense volumes of ash, lava, and gas, the exact timing and duration of this eruption, as well as its environmental and climatic impact remain unclear. Here, we provide a comprehensive chemical analysis of Greenland ice-core records spanning the period 936–943 CE. We identify volcanic ash from at least three different Icelandic eruptions and confirm that there was a major ash and gas emission from Eldgjá in 939 CE. Using tree ring temperature estimates we find strong evidence for Northern Hemisphere climate cooling in the summer of 940 CE. However, the variety of volcanic ash identified in the ice-cores shows that several Icelandic and Northern Hemisphere arc volcanoes were also erupting in this period. While Eldgjá remains the prime candidate, these additional eruptions complicate the attribution of reported climate and societal changes to Eldgjá alone. Ultimately, our study sheds new light on a cluster of volcanic eruptions between 936 and 943 CE and highlights the challenges of disentangling the individual contributions of multiple eruptions on the environment and climate.

HUTCHISON ET AL. 1 of 21

21698996, 2024, 16, Downloaded from https://agupubs.onlinelibrary.wiley.com/doi/10.1029/2023JD040142, Wiley Online Library on [22/08/2024]. See the Terms and Conditions (https://onlinelibrary.wiley

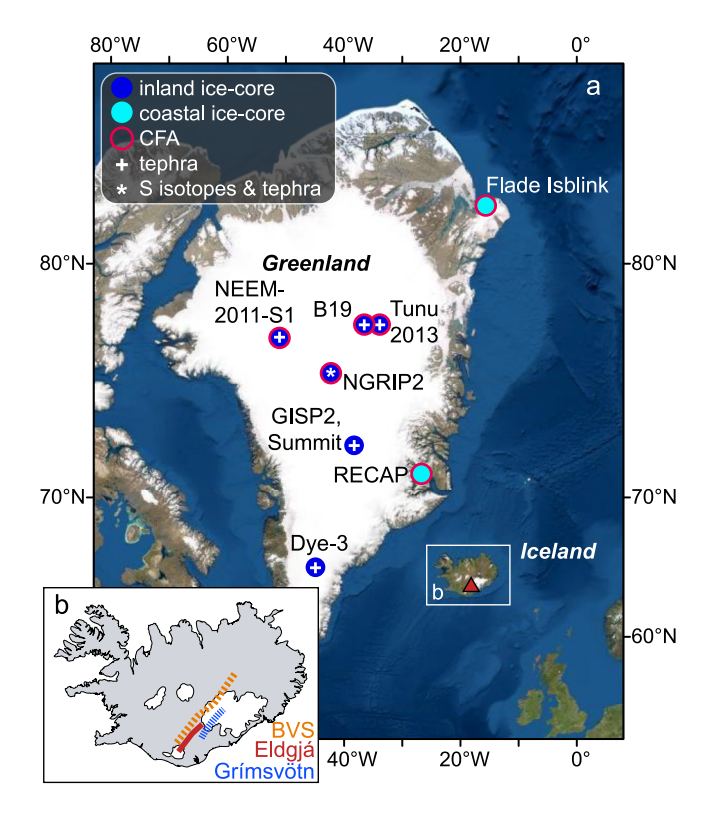


Figure 1. Map (a) showing location of the Eldgjá fissure of Katla system (red triangle), and the Greenland ice-cores referred to in this study (circles). Turquoise circles denote coastal sites, whereas dark blue circles denote inland sites. Ice-cores with high-resolution continuous flow analysis records are outlined in red. Those analyzed for cryptotephra are shown by the white cross, and those with S isotopes and cryptotephra (i.e., NGRIP2) are shown by the asterisk. Inset (b) shows a map of Iceland with the volcanic systems discussed in this study: Eldgjá fissure; Bárdarbunga-Veiðivötn system, and Grímsvötn volcanic system (after Thordarson & Larsen, 2007).

#### 1. Introduction

Large basaltic fissure eruptions emit vast quantities of reactive gases and metals (Ilyinskaya et al., 2017) and can have severe environmental and societal impacts. Iceland's extensional tectonics favor fissure eruptions, and the 1783–1784 Laki eruption (which spanned ~8 months) has become a paradigm for the profound impacts such episodes can have on the environment, climate, and society (Schmidt et al., 2012; Thordarson & Self, 2003; Witham et al., 2015; Zambri et al., 2019). Beyond this particular episode, we have rather sparse knowledge of the episodicity and duration of such large fissure eruptions (>10 km³ of dense products), their volatile yields, atmospheric chemistry and transport of associated plumes, and their climate impacts.

The Eldgjá eruption, associated with Katla volcanic system, is considered the largest Icelandic lava flood, by volume, of the Common Era. This basaltic eruption occurred along a 75-km long fissure (Thordarson & Larsen, 2007) and while dominantly effusive, included at least 16 major subglacial and subaerial explosive episodes (W. M. Moreland et al., 2019). It is estimated to have released 220 Tg of SO2 into the atmosphere (with ~185 Tg of this reaching upper tropospheric and lower stratospheric altitudes, Thordarson et al., 2001). There is no historically-attested date for the eruption but Greenland ice-cores (Figure 1a) revealed a prominent S peak dated to the 930s (Hammer et al., 1980) co-located with basaltic glass shards compatible with Eldgjá's composition (Zielinski et al., 1995). The precise timing of Eldgjá proved controversial. McCarthy and Breen (1997) argued that a blood-red sun recorded in the year 939 CE in the Chronicon Scotorum (Irish Annals) indicated the eruption year, while Stothers (1998) suggested a date of 934 CE based on documentary records of extreme cold and dry fog. The 939 CE event date was later used by Sigl et al. (2015) as a tie-point in their revised chronology for the NEEM-2011-S1 ice-core, and Oppenheimer et al. (2018) confirmed the attribution with reference to the NEEM-2011-S1 highresolution glaciochemistry and the tie point of the 946 CE "Millennium Eruption" of Paektu (China/DPR Korea). Oppenheimer et al. (2018) argued that the eruption was underway by spring of 939 and likely sustained up to

940 CE. They also presented tree-ring reconstructions revealing Northern Hemisphere summer cooling of ~1°C in 940 CE and several medieval sources that attest to climatic anomalies and societal impacts around this time (939–942 CE).

Despite this progress, much remains uncertain about the Eldgjá eruption. For example, Zielinski et al. (1995) also found basaltic andesite, andesite, dacite and rhyolite shards in the "Eldgjá layer" in the GISP2 ice-core, raising the possibility of multiple sources of deposition. Their single ice sample represented a 20 cm section of the core (approximately 1 year) and, significantly, no secondary glass standards were analyzed as part of their automated scanning electron microscopy with energy dispersive spectrometry (SEM-EDS) approach. More recent ice-core studies of Coulter et al. (2012) and Sun et al. (2014) also investigated tephra adjacent to the 939 CE S peak (summarized in Table 1). They identified rhyolitic populations in 938 CE (in Dye-3 ice-core, applying GICC21 timescale revisions of Sinnl et al., 2022; Table 1) and ~940 CE (in NEEM-2011-S1 ice-core). Although these studies corroborated evidence for various silicic eruptions around 938–941 CE they did not reveal further detail concerning the Eldgjá eruption.

The NEEM-2011-S1 record also reveals complexity in the volatile tracers (including trace metals) that has not been explained (Oppenheimer et al., 2018), and without constraints on the transport and chemistry of the emissions from Eldgjá (notably injection height of sulfur) attributing surface cooling signal to the eruption is tenuous. A further uncertainty of the Eldgjá eruption is its overall duration. Thordarson et al. (2001) proposed a minimum duration of 6 months based on lava cooling considerations and a 3 to 6-year duration based on early Greenland ice-core acidity records (from GISP2 and Crete, Hammer, 1984; Zielinski et al., 1995). Oppenheimer et al. (2018) suggested a short, ~1.5-year duration based on the S and Cl records from the sub-annually resolved

HUTCHISON ET AL. 2 of 21



Summary of Key Tephra Deposits Spanning the Period of Study

Tephra	Composition(s)	Locations found	Age [depth ice]	Source(s)	Key references
Eldgjá	Transitional alkali and tholeiitic basalt	South-central Iceland	939 CE	Eldgjá fissure, Iceland	Larsen (2000), Thordarson et al. (2001), Schmid et al. (2017), W. M.Moreland et al. (2019), and Oppenheimer et al. (2018)
V-Sv	Tholeiitic basalt	North Iceland	938 ± 6 CE	Bárðarbunga- Veiðivötn system, Iceland? (based on geochemistry)	Lawson et al. (2007), Sigurgeirsson et al. (2013), Schmid et al. (2017), and Hiles et al. (2021)
Grímsvötn	Tholeiitic basalt	South Iceland	~919–939 CE <sup>†</sup>	Grímsvötn system	Óladóttir, Larsen, and Sigmarsson (2011)
Grímsvötn	Tholeiitic basalt	South Iceland	$\sim$ 939 $-$ 969 CE $^{\dagger}$	Grímsvötn system	Óladóttir, Larsen, and Sigmarsson (2011)
MOR-T4	Rhyolite and dacite	UK, Ireland	937 ± 10 CE	Unknown	Chambers et al. (2004), Watson et al. (2016, 2017), and Plunkett et al. (2023)
SB-4	Rhyolite	North America	~875–995 CE	Fish Lake II; Chaos Crags, Lassen Peak, USA? (based on geochemistry)	Clynne et al. (2008), Foit and Mehringer (2016), and Jensen et al. (2021)
Jala Pumice	Rhyolite	North America, Ireland	~890-1130 CE	Volcan Ceboruco, Mexico	Gardner and Tait (2000), Sieron and Siebe (2008), Mackay et al. (2016), Plunkett and Pilcher (2018), and Jensen et al. (2021)
Glass-A	Basalt and basaltic andesite	Greenland, GISP2	939–940 CE (*938 CE) [272.20– 272.42 m]	Eldgjá fissure, Iceland, and unknown	Zielinski et al. (1995)
Glass-B	Dacite	Greenland, GISP2	939–940 CE (*938 CE) [272.20– 272.42 m]	Unknown	Zielinski et al. (1995)
QUB-1212/13	Rhyolite	Greenland, Dye-3	938 CE (*931 CE) [494.45– 494.85 m]	Unknown	Coulter et al. (2012)
QUB-1823	Rhyolite	Greenland, NEEM- 2011-S1	939–940 CE [248.53– 248.70 m]	Unknown	Sun et al. (2014)

Nore. Note that for the GISP2 and DYE-3 tephras we show the original published age (\*) and the revised ice-core age (see Section 1). The ages of the Grímsvötn eruptions (') are approximate and are based on their occurrence above and below the Eldgiá tephra and their calculated soil accumulate rate ages from Oladóttir, Larsen, and Sigmarsson (2011).

2169896, 2024, 16, Downloaded from https://agupubs.onlinelibrary.wiley.com/doi/10.109/2023JD40142, Wiley Online Library on [22/08/2024]. See the Terms and Conditions (https://onlinelibrary.wiley.com/terms-and-conditions) on Wiley Online Library for rules of use; OA articles are governed by the applicable Cerative Commons Licenses

HUTCHISON ET AL. 3 of 21

NEEM-2011-S1 ice-core. These uncertainties have implications for estimating time-averaged eruption intensities, and for considering environmental consequences of tephra and volatile emission.

Local and regional tephra records in soil and sedimentary sequences provide additional constraints on the magnitude and timing of volcanism around the period of the Eldgjá eruption. In Iceland, Eldgjá tephra dominates in south-central Iceland with a major dispersal toward the south-east and less prominent dispersal toward the north-west (Larsen, 2000). Although these deposits are dominantly of transitional alkali basalt composition (Larsen, 2000), Thordarson et al. (2001) noted that clasts of tholeiitic basalt occur throughout the Eldgjá tephra sequence. W. M. Moreland et al. (2019) referred to these as hyaloclastite fragments and while they generally account for <5 modal % of the deposit, in the most northerly sections of the fissure these tholeiitic clasts become dominant (Thordarson et al., 2001). Eldgjá tephra is not found in the north of Iceland, but a distinctive tholeiitic basalt tephra, V-Sv, is identified over large parts of north Iceland and has been dated to 938  $\pm$  6 CE (using sediment accumulation rates and the Greenland ice-core date for the underlying Landnám tephra layer, Sigurgeirsson et al., 2013; Schmid et al., 2017). Based on its geochemistry, V-Sv has been attributed to the Bárðarbunga-Veiðivötn system which is located to the north of the Eldgjá fissure (Figure 1b). There are no sites where Eldgjá and V-Sv tephra are preserved together, and so the stratigraphic relationship between these two eruptions remains unresolved.

Tholeitic activity is also known to have occurred in the Reykjanes peninsula in the 10th century (Sæmundsson et al., 2016) and around the Vatnajökull ice cap in south-central Iceland where two additional tholeitic basalt tephra layers bracket Eldgjá tephra in soil sections (Óladóttir, Larsen, & Sigmarsson, 2011; Figure 1b and Table 1). The precise timing of these tephra layers is not known, although ages based on soil accumulation rate suggest they pre- and post-date Eldgjá by as little as a few years. Their exact source and dispersal is unconstrained but based on geochemistry they are attributed to the Grímsvötn volcanic system (north of the Eldgjá fissure and adjacent to the Bárðarbunga-Veiðivötn system, Óladóttir, Larsen, & Sigmarsson, 2011; Figure 1b and Table 1). Resolving the precise timing of Eldgjá and eruptions of Bárðarbunga-Veiðivötn and Grímsvötn is important for Icelandic tephrochronology. It is also vital to constrain their eruptive style, magnitude, and altitude of S emissions, as it allows us to understand whether long duration fissure eruptions (i.e., Eldgjá) or short duration phreatoplinian eruptions (typical of Grímsvötn and Bárðarbunga-Veiðivötn) are more climatically significant.

Eldgjá tephra fallout has yet to be found in Europe or North America but there are numerous contemporary silicic tephra deposits that date approximately to this time (Table 1). In Europe, the period of ~937 ± 10 CE is represented by the MOR-T4 tephra (first identified in An Loch Mór, western Ireland, by Chambers et al., 2004). MOR-T4 has been found at numerous sites in the UK and Ireland and comprises several populations of rhyolitic and dacitic composition (Plunkett & Pilcher, 2018; Plunkett et al., 2023; Watson et al., 2016, 2017). Several shards from MOR-T4 in Faddanmore, Ireland, overlap geochemically with the rhyolitic Jala Pumice tephra (Volcan Ceboruco, Mexico; Plunkett & Pilcher, 2018). Cryptotephra from peatlands in north-eastern North America also reveal numerous silicic populations spanning circa 890–1130 CE. One of these has been also attributed to the Jala Pumice (Mackay et al., 2016), while another (SB-4), found co-mingled with Jala, has been tentatively linked to Lassen Volcanic Center in the Cascades (Jensen et al., 2021). The salient point is that numerous silicic tephra populations have been identified and dated to ~930–950 CE (i.e., spanning the Eldgjá eruption), yet few robust correlations have been made. Constraining the timing of these silicic eruptions, together with the mafic Icelandic eruptions mentioned above, is important and allows us to elucidate which eruption(s) may have triggered climatic and societal impacts or, possibly, combined to increase such impacts.

Given that there is limited scope for textual sources to illuminate further the nature and impacts of the Eldgjá eruption, and that stratigraphic and sedimentological work on the proximal deposits will struggle to achieve precise geochronological control, high-temporal resolution analysis of well-dated ice-cores (Oppenheimer et al., 2018) arguably offers the most promising means to shed new light on this period of volcanic activity. First, continuous flow analysis (CFA) of ice-cores can yield precisely dated, sub-annual records of volcanic fallout including S, Cl, trace metals, and particles (McConnell et al., 2017; Sigl et al., 2015). Second, sulfur isotopes of ice-core sulfate can constrain the approximate injection height of volcanic emissions since SO<sub>2</sub> exposed to UV radiation in and above the stratospheric ozone layer acquires a sulfur mass-independent fractionation signature (Baroni et al., 2007; Burke et al., 2019; Gautier et al., 2019; Savarino et al., 2003). And third, the particle records generated by CFA can reveal time lags between tephra and volatile deposition (which relate to atmospheric

HUTCHISON ET AL. 4 of 21

21698996, 2024, 16, Downloaded from https://agupubs.onlinelibrary.wiley.com/doi/10.1029/2023JD040142, Wiley Online Library on [22/08/2024]. See the Terms and Condition

transport) and permit targeted sub-sampling of tephra populations for geochemical fingerprinting (McConnell et al., 2017, 2020; Plunkett et al., 2023).

Our aims here are to use such a multi-pronged glaciochemical analysis to improve understanding of Northern Hemisphere volcanism between 936 and 943 CE, and resolve the distinct volcanic contributions to the ice-core deposition signal, thereby enabling exploration of links (if any) between eruptions and environmental, climatic, and societal change.

#### 2. Methods

#### 2.1. Glaciochemistry

Ice-core locations referred to in this study can be broadly divided into inland (NEEM-2011-S1, Tunu2013, B19, NGRIP2, GISP2, Summit, Dye-3) and coastal (Flade Isblink, RECAP) locations (Figure 1a). Chemical and elemental records, as well as particle concentration measurements were made at the Ultra Trace Chemistry Laboratory at the Desert Research Institute (DRI) and are available for all cores except GISP2, Summit, and Dye-3. The details of the setup, which includes two High Resolution Inductively Coupled Plasma Mass Spectrometers (HR-ICP-MS) operating in parallel for simultaneous elemental measurements of S, Cl, Na, Cd, and other metals, are provided by Sigl et al. (2015) and McConnell et al. (2017).

S and Cl mainly originate from volcanic and marine sources and were corrected to non-sea-salt S and Cl, nssS and nssCl, respectively, using precisely co-registered measurements of Na and Ca. Peaks in insoluble particle concentrations are often associated with cryptotephra (Plunkett et al., 2020, 2023). These were measured optically in two size ranges, 2.6–4.5 µm and 4.5–9 µm, and were used to guide sub-sampling for cryptotephra (Section 2.3). Timescales for all the ice-core records except Flade Isblink were established by annual layer counting of seasonal cycles in chemical impurities and water isotopes on the DRI-NGRIP2 chronology, and further constrained by recognized volcanic marker horizons (McConnell et al., 2018). This age scale shows good agreement with the earlier NEEM-2011-S1 chronology (Sigl et al., 2015) with both chronologies placing the main S emission at 939 CE. At the Flade Isblink site, extensive surface melting, percolation, and refreezing, as well as very high concentrations of sea-salt and other marine inputs, preclude clear annual layer identification, so only volcanic marker synchronization was used. For all sites, the chronologies are based on synchronization of the prominent 939 CE S peak with the absolute date of the fallout established using the annually resolved NGRIP2 and NEEM-2011-S1 records.

#### 2.2. Multiple Sulfur Isotopes

S isotopes ( $^{34}$ S,  $^{33}$ S, and  $^{32}$ S) were measured on sub-samples of the NGRIP2 ice-core by MC-ICP-MS (detailed procedures are given by Burke et al., 2019). In brief, 20 discrete samples were cut over a depth of 220.55–219.45 m corresponding to 936–941 CE at a nominal 2–3-month resolution. Sulfate concentration was measured by ion chromatography and 10–20 nMol of sulfate was extracted via column chemistry (Burke et al., 2019). An inhouse secondary standard, Switzer Falls river water (Burke et al., 2018), and procedural blanks were also passed through columns and prepared for isotope analysis. Isotopic analysis was performed using a Neptune Plus MC-ICP-MS at the University of St Andrews in two sessions in December 2020 and February 2021. Switzer Falls had  $\delta^{34}$ S of 4.12%  $\pm 0.13\%$  and  $\Delta^{33}$ S of -0.02%  $\pm 0.08\%$  (2 s.d., n = 13), consistent with previous measurements by Burke et al. (2018, 2019) and Crick et al. (2021). Procedural blanks contained 0.21  $\pm$  0.09 nMol S and had  $\delta^{34}$ S of 4.98%  $\pm 1.49\%$  (2 s.d., n = 6). These values are comparable with the aforementioned studies and were used to blank correct all measurements.

As part of our S isotope analytical procedure, we also analyze large ( $\sim$ 30 cm,  $\sim$ 0.5–1 year) background samples from NGRIP to constrain natural variability in periods unaffected by major volcanic events. Using isotope mass balance, it is then possible to determine endmember isotope values of the volcanic sulfate emissions ( $\delta_{\rm volc}$ ) using the following expression from Baroni et al. (2007):

$$\delta_{\text{volc}} = (\delta_{\text{meas}} - f_{bkod}\delta_{bkod})/f_{\text{volc}} \tag{1}$$

where  $\delta_{\text{meas}}$  and  $\delta_{bkgd}$  are the  $\delta^{34}$ S or  $\delta^{33}$ S of the measured and background values, respectively.  $f_{bkgd}$  is the mass fraction of the total sulfate in the background ( $f_{bkgd} = [SO_4]_{bkgd}/[SO_4]_{sample}$ ), and  $f_{\text{volc}}$  is the mass fraction of

HUTCHISON ET AL. 5 of 21

21698996, 2024, 16, Downloaded from https://agupubs.onlinelibrary .com/doi/10.1029/2023JD040142, Wiley Online Library on [22/08/2024]. See the Terms and Condition

volcanic sulfate ( $f_{\text{volc}} = 1 - f_{bkgd}$ ). Following Gautier et al. (2018) and Burke et al. (2019), we only plot  $\delta_{\text{volc}}$  for samples with greater than 65% volcanic sulfate ( $f_{\text{volc}} > 0.65$ ).

#### 2.3. Cryptotephra

Melted ice-core sub-samples were centrifuged and then concentrated on microprobe slides (NGRIP2) or stubs (B19, GISP2, Tunu2013). For NGRIP2, the same sub-samples were used for both S isotopes and cryptotephra (i.e., after centrifuging, all but the bottom 2-3 ml of supernatant was removed for isotope analysis and the remainder used for cryptotephra sampling). For NGRIP2 and B19, glass shards were identified using optical microscopy. For GISP2 and Tunu2013, shards were examined using a combination of optical microscopy and SEM-EDS (using a JEOL JXA-iSP100 at the University of St Andrews). Once particles were identified, the slides and stubs were polished and major element analyses were performed over several EPMA sessions at the University of Bern and Queen's University Belfast, using a 5 µm beam, and at the University of St Andrews, using a 3 and 5 µm beam. Full details of the operating conditions are given in Supporting Information S1. In addition to the ice-core samples we also analyzed proximal tephra from south of the Eldgiá fissure (detailed in Data Set S3). These were analyzed at Bern and St Andrews using similar operating conditions to the unknowns. For each session a range of international secondary glass standards from Kuehn et al. (2011) and Jochum et al. (2006) were analyzed throughout the run to evaluate instrumental accuracy and precision. Most ice-core shards gave analytical totals >95% (Data Set S3). Some shards from Tunu2013 and GISP2 were ≤5 µm, which made them difficult to polish and too small for a 3 µm beam. As a result, these gave analytical totals of 60%–90%, and so to compare all EPMA data we normalized all totals to 100% on an anhydrous basis. Despite their low analytical totals these shards yielded consistent geochemical populations which are detailed in Section 3.3.

#### 3. Results

#### 3.1. Glaciochemical Records

Glaciochemical records of inland cores are shown in Figure 2. All cores show a pronounced S peak in mid-939 CE followed ~6 months later by a peak in Cl and volatile metals (e.g., Cd). In all inland cores, S shows several shoulders following the peak value in mid-939 CE (Figure 2). Another notable feature is that while B19 and Tunu2013 show an increase in S through 936–939 CE, NGRIP2 and NEEM-2011-S1 show only a couple of subtle (<50 ng/g) S peaks before the rapid increase in 939 CE. Although relatively minor compared to the main 939 CE S peak, there is evidence from both S isotopes and cryptotephra that these subtle pre-939 CE S peaks do have a volcanic origin (developed in Sections 3.2 and 3.3). Chemical records from the inland cores also show a spatial correspondence. B19 and Tunu2013 are just ~60 km apart and are more easterly and lower in elevation than NGRIP2 and NEEM-2011-S1 (Figure 1a). The ice-cores that are closest to each other (i.e., B19 and Tunu2013) record similar S deposition patterns (i.e., increasing S concentrations through 936–939 CE). Insoluble particle concentrations (which include dust and tephra) are available for all cores except NEEM-2011-S1 (Figure 2). These data show multiple particle peaks throughout this period, and while there is some variability between cores all reveal peaks in 937, 940, and 941 CE.

CFA records from coastal sites are shown in Figure 3. These sites are more influenced by marine sources and for Flade Isblink sea-salt corrections yield complex patterns (particularly in Cl), and so for clarity we plot the measured S and Cl values (i.e., not corrected for sea-salt contribution), which can be compared with typical background values observed in 934–935 CE. RECAP and Flade Isblink both show a major S peak in 939 CE. Cl is highly elevated at coastal sites, and both records show significant peaks in Cd. Peaks in Cl and Cd are co-located with the peak in S, in contrast to the delayed peaks observed at inland sites (Figure 2). Na, shown in Figure S1 in Supporting Information S1, is also highly elevated at coastal sites with peak values in 940 CE. Particle records are also more variable at coastal sites. At Flade Isblink there are multiple peaks throughout 935–937 CE and smaller peaks from 939 to 942 CE. At RECAP, the most prominent peak is in late 939 CE (co-located with the S, Cl, and Cd anomalies, Figure 3), but there are subsidiary peaks in 937 and 938 CE. As with the inland sites, there are indicators of volcanic activity prior to 939 CE, most notably a large (~2,000 ng/g) Cl peak in 938 CE registered at Flade Isblink. Finally, a large Cd peak is also noted in Flade Isblink at 936 CE but unlike the late 939 CE peak there is no corresponding deposition of S and Cl. In a volcanic plume Cd would most likely form a soluble chloride aerosol and one would expect these two species to deposit together (Mason et al., 2022). Though we did

HUTCHISON ET AL. 6 of 21

2169896, 2024, 16, Downloaded from https://agupub.son/inelibrary.wiley.com/doi/10.1029/2023JD00142, Wiley Online Library on [22/082024]. See the Terms and Conditions (https://onlinelibrary.wiley.com/terms-and-conditions) on Wiley Online Library for rules of use; OA articles are governed by the applicable Creative Commons Licenses

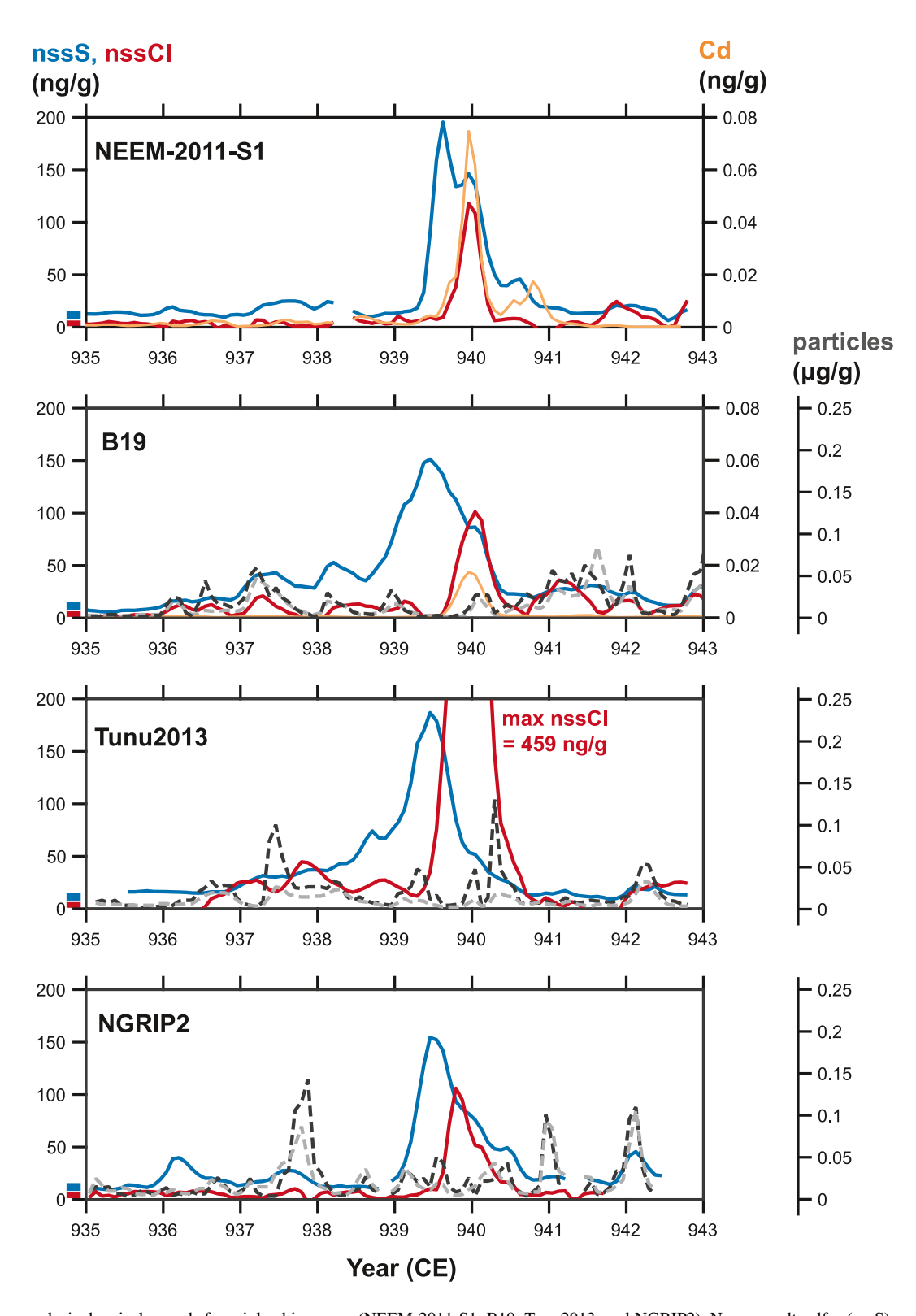


Figure 2. Continuous glaciochemical records from inland ice-cores (NEEM-2011-S1, B19, Tunu2013, and NGRIP2). Non-sea salt sulfur (nssS) and chlorine (nssCl) concentrations (in ng/g) are shown on the left-hand axis, while cadmium (Cd in ng/g) and insoluble particle concentrations (i.e., dust and tephra, in  $\mu$ g/g) are shown on the right-hand axis. For NEEM-2011-S1 particle concertation data are unavailable, as was Cd in Tunu2013 and NGRIP2. Note that for particles the darker dashed line shows the 4.5–9.5  $\mu$ m size fraction while the light dashed line shows particles in the 2.6–4.5  $\mu$ m fraction. Typical non-volcanic background values for nssS and nssCl from a stack (N=6) of Greenland ice-cores (after Gabriel et al., 2024) are shown by the blue and red bars on the left-hand axis.

HUTCHISON ET AL. 7 of 21

2169896, 2024, 16, Downloaded from https://agupub.son/inelibrary.wiley.com/doi/10.1029/2023JD00142, Wiley Online Library on [22/082024]. See the Terms and Conditions (https://onlinelibrary.wiley.com/terms-and-conditions) on Wiley Online Library for rules of use; OA articles are governed by the applicable Creative Commons Licenses

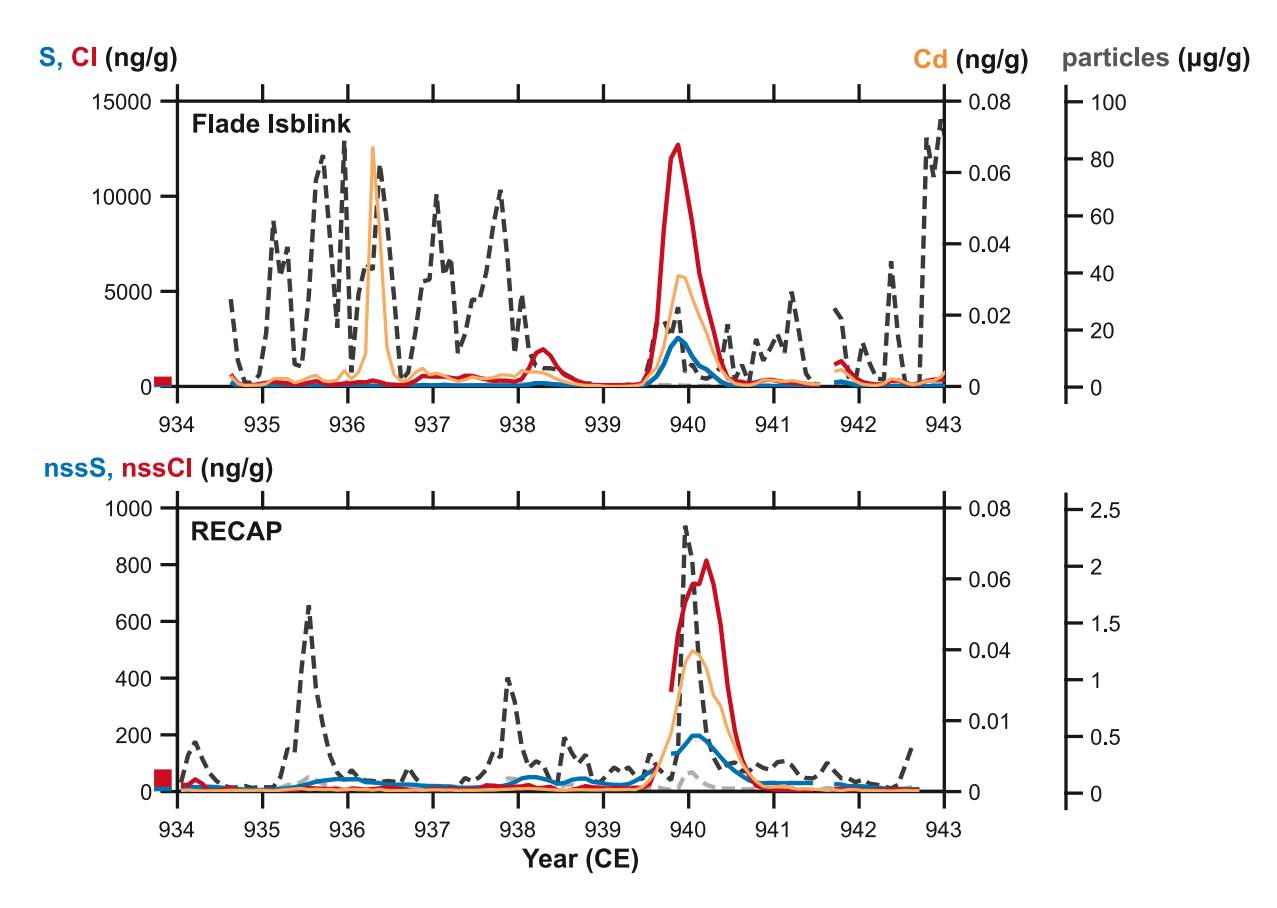


Figure 3. Continuous glaciochemical records from coastal ice-cores (Flade Isblink and RECAP). For RECAP non-sea salt sulfur (nssS) and chlorine (nssCl) concentrations (in ng/g) are shown on the left-hand axis. For Flade Isblink the measured S and Cl values are shown because this site is strongly influenced by marine sources and sea-salt corrections often yield complex patterns (particularly in Cl). Cadmium (Cd in ng/g) and particles (i.e., dust and tephra, in  $\mu g/g$ ) are shown on the right-hand axes. Note that the darker dashed line shows particles in the  $4.5-9.5~\mu m$  size fraction while the light dashed line shows particles in the  $2.6-4.5~\mu m$  fraction. Typical non-volcanic background values for nssS and nssCl are shown by the blue and red bars on the left-hand axis. Note that while both RECAP and Flade Isblink are coastal sites, their elevations are markedly different (2.340~m) and 618~m, respectively). As a result, Flade Isblink is more strongly influenced by marine aerosols and coastal dust and has far greater concentrations of S, Cl, and particles. Particle peaks in Flade Isblink between 935 and 938 CE are most likely related to coastal dust rather than tephra, though we have not performed tephra extracts on these sections of ice (see Methods).

not extract particles from any of the Flade Isblink samples the lone Cd peak at 936 CE (without elevated Cl) suggests a non-volcanic origin (although this hypothesis warrants further investigation).

#### 3.2. Sulfur Isotopes

Sulfur concentrations,  $\delta^{34}$ S and  $\Delta^{33}$ S of sub-samples from NGRIP2 are shown in Figures 4a–4c. Measured  $\delta^{34}$ S ranges between -0.5% and 8.2%, with the lowest values for the samples immediately preceding the 939 CE S peak. Measured  $\Delta^{33}$ S varies between -0.4% and 0.2% with most samples showing values that are analytically indistinguishable from zero (considering the observed 2 s.d. variation for our non-MIF Switzer Falls standard, Section 2.2).

Background S concentrations and  $\delta^{34}$ S in NGRIP are  $21 \pm 5$  ng/g and  $8.2\% \pm 1.3\%$ , respectively (based on seven,  $\sim$ 1 year samples, with ages between  $\sim$ 1600 BCE and 1800 CE, Data Set S2). These background values are comparable to S concentrations ( $10 \pm 6$  ng/g) and  $\delta^{34}$ S of ( $9.7\% \pm 2.8\%$ ) measured at Summit ice-core in years without large volcanic eruptions (Jongebloed et al., 2023). Almost all our samples have higher S (30–190 ng/g) and lower  $\delta^{34}$ S (between -0.5% and 5.7%) compared to typical background, indicating an enhanced volcanic S flux over the whole 936–940 CE period (increased marine contributions are precluded because they would result in a high  $\delta^{34}$ S of  $\sim$ 18% $_{0}$ –21% $_{0}$ ; Patris et al., 2000; Jongebloed et al., 2023). Even though none of our 936–940 CE samples represent non-volcanic background values, we can use our compilation of NGRIP background samples to evaluate isotope values of the volcanic endmember (Equation 1). These data are shown by the white filled

HUTCHISON ET AL. 8 of 21

21698996, 2024, 16, Downloaded from https://agupubs.onlinelibrary.wiley.com/doi/10.1029/2023JD040142, Wiley Online Library on [22/08/2024]. See the Terms and Condition

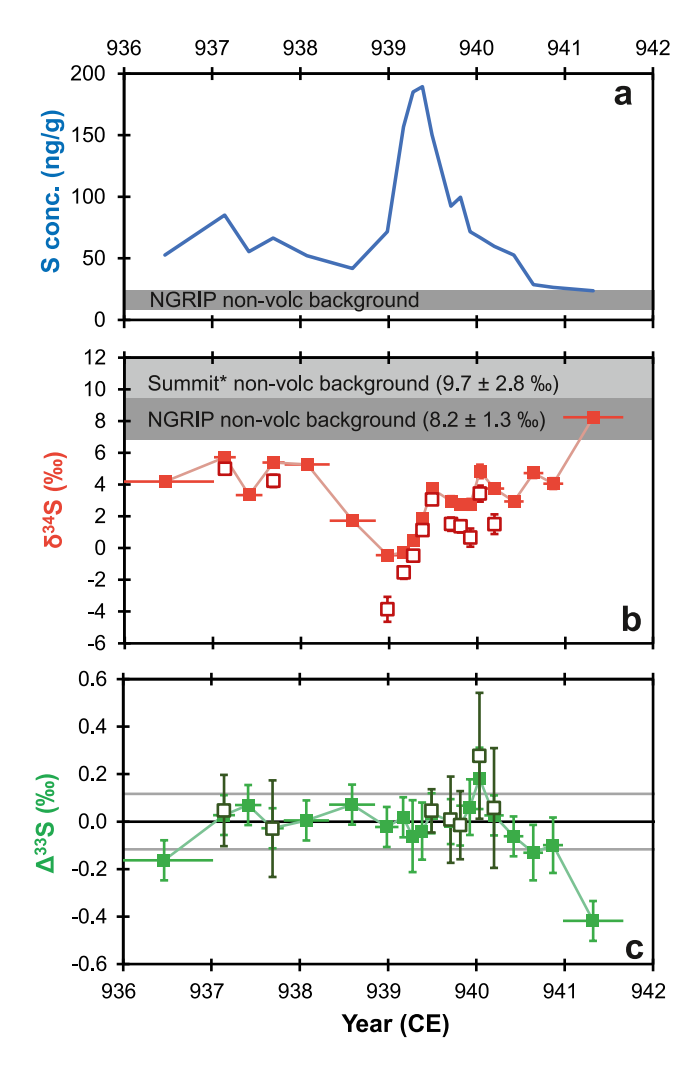


**Figure 4.** Sulfur concentration (a),  $8^{34}$ S (b), and  $\Delta^{33}$ S (c) from NGRIP2 for the 936–942 CE period. In (b) and (c) the red and green filled symbols are measured values. The unfilled red and green symbols are background corrected volcanic  $8^{34}$ S and  $4^{33}$ S (for samples with >65% volcanic sulfate, Section 3.2). In (a) and (b) gray bars denote S concentration and  $4^{34}$ S in non-volcanic background years from Summit ice-core (after Jongebloed et al., 2023) and NGRIP (this study). In (c) the gray lines show the 2 s.d. values of our non-MIF ( $4^{34}$ S) Switzer Falls river water standard (Section 2.2).

symbols in Figures 4b and 4c, and while they make only a small change to  $\Delta^{33}$ S, they highlight the extremely low  $\delta^{34}$ S of the volcanic endmember (down to -3.9%).

Finally, most of the  $\Delta^{33}$ S values are indistinguishable from 0‰, indicating aerosol transport below the stratospheric ozone layer, that is, in the upper troposphere or lower stratosphere (Burke et al., 2019; Savarino et al., 2003). Importantly, several samples in 940–941 CE have small non-zero  $\Delta^{33}$ S values and are discussed in detail in Section 4.3.

#### 3.3. Cryptotephra

We extracted and chemically analyzed 70 shards from NGRIP2, GISP2, B19 and Tunu2013 (typical morphologies are shown in Figure S2 in Supporting Information S1). Our sub-sampling specifically targeted particle peaks and in Figure 5b we provide the age range of each cryptotephra sub-sample from this study and previous work. Nominal time resolution of the sub-samples varies between ~2 months (GISP2) to ~1.5 years (Tunu2013). Gaps in the time series (e.g., in B19 ~938-940 CE) reflect the fact that in these periods no tephra was found using optical microscopy and therefore no EPMA data were acquired. A long-running question in the ice-core cryptotephra community is whether remobilized ash from continental areas could be redeposited at the high-altitude locations sampled by the Greenland ice-cores. Plunkett et al. (2020) concluded that in Greenland re-mobilized shards are likely to be extremely rare. Nevertheless, we decided to apply an additional screening of our data by excluding tephra populations with normalized Na<sub>2</sub>O values <1 wt. % (since Na is one of the first elements to be leached by meteoric fluids, Cerling et al., 1985, and geochemical analysis of fresh glasses usually show Na<sub>2</sub>O values >>1 wt.%). With the exception of seven basaltic andesite shards from NGRIP2, all shards had sufficiently high Na<sub>2</sub>O values and are assumed to be representative of primary ash fall. Our full data set (which includes tephra geochemistry, depths and ages) is provided in Data Set S3. We note that there are rare outliers (e.g., the two high CaO analyses from B19, Data Set \$3) but we focus our attention on the samples that show populations of tephra with distinct geochemical clusters.

Given the large number of tephra shards it is helpful to broadly divide the samples into two temporal groups: early (936–940 CE), and late (940–942 CE) with the division marked by the Cl peak which occurs in all data sets at the end of 939 CE (Figure 5a). In the early tephra (Figures 5b and 5d), we find basaltic shards in our samples from B19 and NGRIP2. In the late tephra (Figures 5b and 5e), we also see a population of basaltic shards as well as shards of basaltic andesite, dacite and rhyolite compositions. These are

broadly consistent with the variety reported by Zielinski et al. (1995) in GISP2, and reinforce the picture of contemporaneous deposition from multiple volcanic sources (note that we do not show the Zielinski et al., 1995 data in Figure 5 for the sake of clarity and because they employed a standardless automated SEM-EDS method that is not readily compared with modern EPMA).

In Figure 6 we compare the chemistry of the basaltic shards with glass analyses for proximal Icelandic eruption products known to have occurred within the timeframe of interest. Our samples of proximal Eldgjá tephra (Data Set S3) compare well with previous analyses of the transitional alkali basalt and we note that no tholeitic basalt was identified (not wholly surprising given we targeted sites south of the fissure where tholeitic clasts are only a minor component, <5 modal %, W. M. Moreland et al., 2019). In all plots, the Eldgjá transitional alkali basalt (which represent the bulk of the Eldgjá fissure products) is represented in a low SiO<sub>2</sub> cluster (with distinct high FeO and TiO<sub>2</sub> values). A number of ice-core shards from GISP2 and NGRIP2 overlap these transitional alkali basalt chemistries and confirm the timing of the Eldgjá eruption between 939 and 940 CE.

HUTCHISON ET AL. 9 of 21

2169896, 2024, 16, Downloaded from https://agupub.son/inelibrary.wiley.com/doi/10.1029/2023JD404142, Wiley Online Library on [22/082024]. See the Terms and Conditions (https://onlinelibrary.wiley.com/terms-and-conditions) on Wiley Online Library for rules of use; OA articles are governed by the applicable Creative Commons Licensia

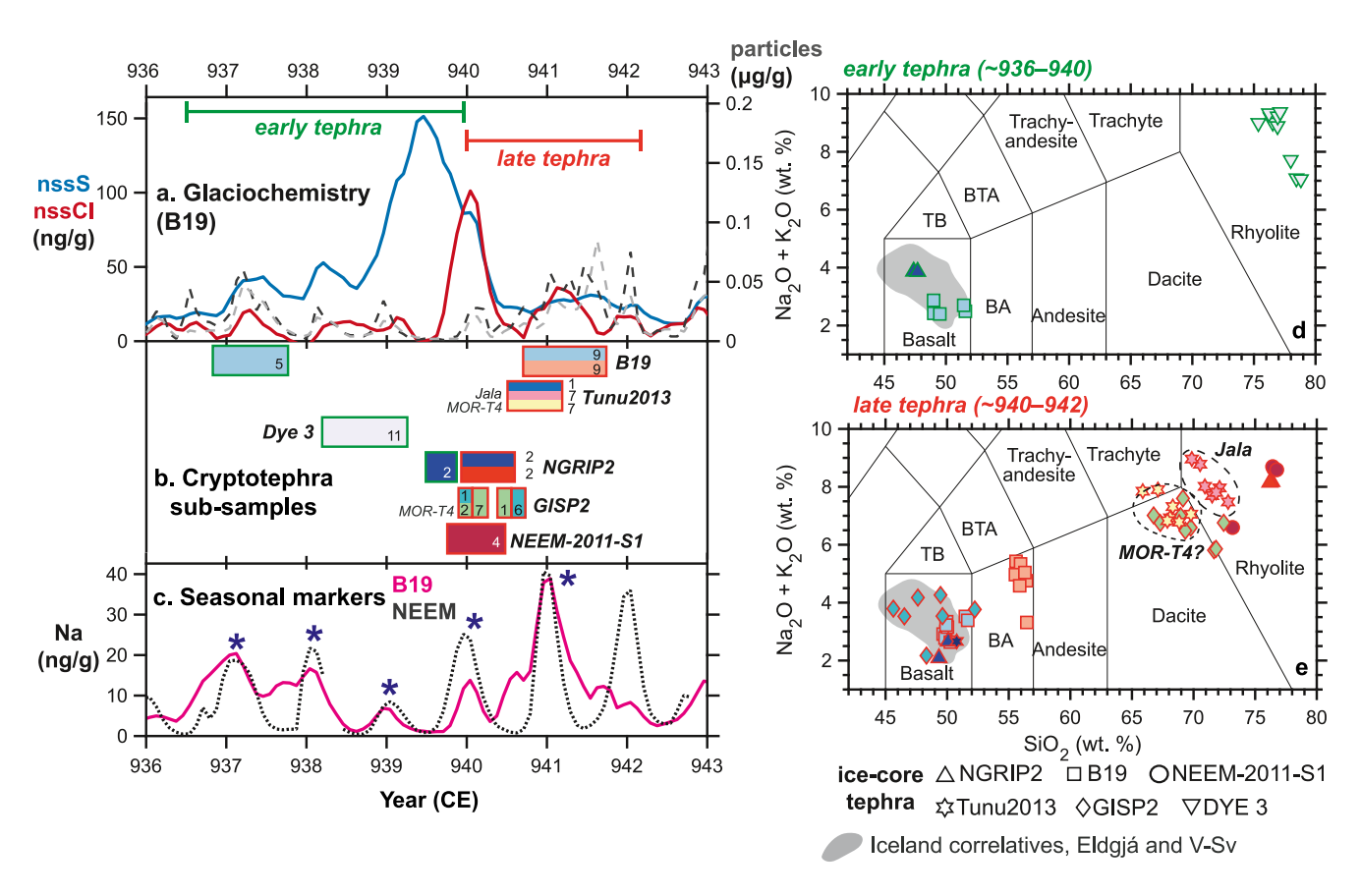


Figure 5. Timeseries of glaciochemistry and summary of cryptotephra populations identified. The top panel of the left-hand plot (a) shows non-sea-salt sulfur (nssS) and chlorine (nssCl) concentrations (in ng/g) and particles (in  $\mu$ g/g) from B19 core. Note that for particles the darker dashed line shows the 4.5–9.5  $\mu$ m size fraction while the light dashed line shows particles in the 2.6–4.5  $\mu$ m fraction. The rectangles in the middle panel (b) show the time resolution of all cryptotephra sub-samples containing glass shards. The number of shards analyzed are shown and the colors correspond to the geochemistry in the total alkali silica plots on the right-hand diagram (d, e). We divide the tephra into two groups: early tephra (936–940 CE, green outlines) and late tephra (940–942 CE, red outlines) (with the division marked by the end-939 CE Cl peak). In the lower panel (c) we show Na concentrations (in ng/g) from B19 and Tunu2013, with annual cycles shown by the blue asterisk. In the right-hand plots (d, e) we show the geochemistry of the different early (green outline) and late (red outline) tephra populations. The symbols correspond to the different ice-cores. Icelandic correlatives are shown by the gray shaded region and identified silicic populations (MOR-T4 and Jala, discussed in the text) are outlined by dashed circles.

Tholeitic basalt tephra with higher  $SiO_2$ , lower  $TiO_2$ , and a range of other major element concentrations are found in both ice-core and proximal localities (Figure 6). Focusing on the proximal tephra, and the known Icelandic eruptions spanning the period of study (Table 1), the V-Sv and Grímsvötn tephras are readily discriminated by their  $TiO_2$ , CaO, MgO, and  $FeO_t$ , A plot of  $FeO_t$  versus  $TiO_2$  is commonly used to distinguish between Grímsvötn and Bárðarbunga-Veiðivötn glasses such as V-Sv (Óladóttir, Sigmarsson, et al., 2011), and we note that the tholeitic basalt clasts within the Eldgjá tephra show a range of compositions that match both fissure systems. Thus, proximal records could indicate that Grímsvötn and Bárðarbunga-Veiðivötn tephra are incorporated into the Eldgjá deposit, indicating eruptions at these systems at the same time as Eldgjá.

The tholeiitic tephra in the ice-core samples also overlap with both Grímsvötn and Bárðarbunga-Veiðivötn (V-Sv) glass populations (Figure 6). Bárðarbunga-Veiðivötn chemistries are found in the early tephra, while both compositions are found in the late tephra. These data clearly reveal a protracted period of Icelandic volcanism from multiple fissure systems. Notably, core B19 (an inland site) resolves the fallout of tholeiitic basalt tephra to have occurred both well before and well after the main 939 CE peak, spanning ~936–941 CE (Figure 5b). As an additional test of the reliability of our age model we examined seasonal peaks in Na which show multiple annual cycles (shown by the asterisks in Figure 5c) supporting a ~4-year duration for this span of fallout. Importantly, basaltic tephra were not found in every sub-sample (e.g., GISP2 in Figure 5a) likely reflecting vagaries of synoptic meteorology, plume heights and trajectories of the various phases of the different eruptions.

HUTCHISON ET AL. 10 of 21

2169896, 2024, 16, Downloaded from https://agupub.son/inelibrary.wiley.com/doi/10.1029/2023JD040142, Wiley Online Library on [22/082024]. See the Terms and Conditions (https://onlinelibrary.wiley.com/terms-and-conditions) on Wiley Online Library for rules of use; OA articles are governed by the applicable Creative Commons Licensen

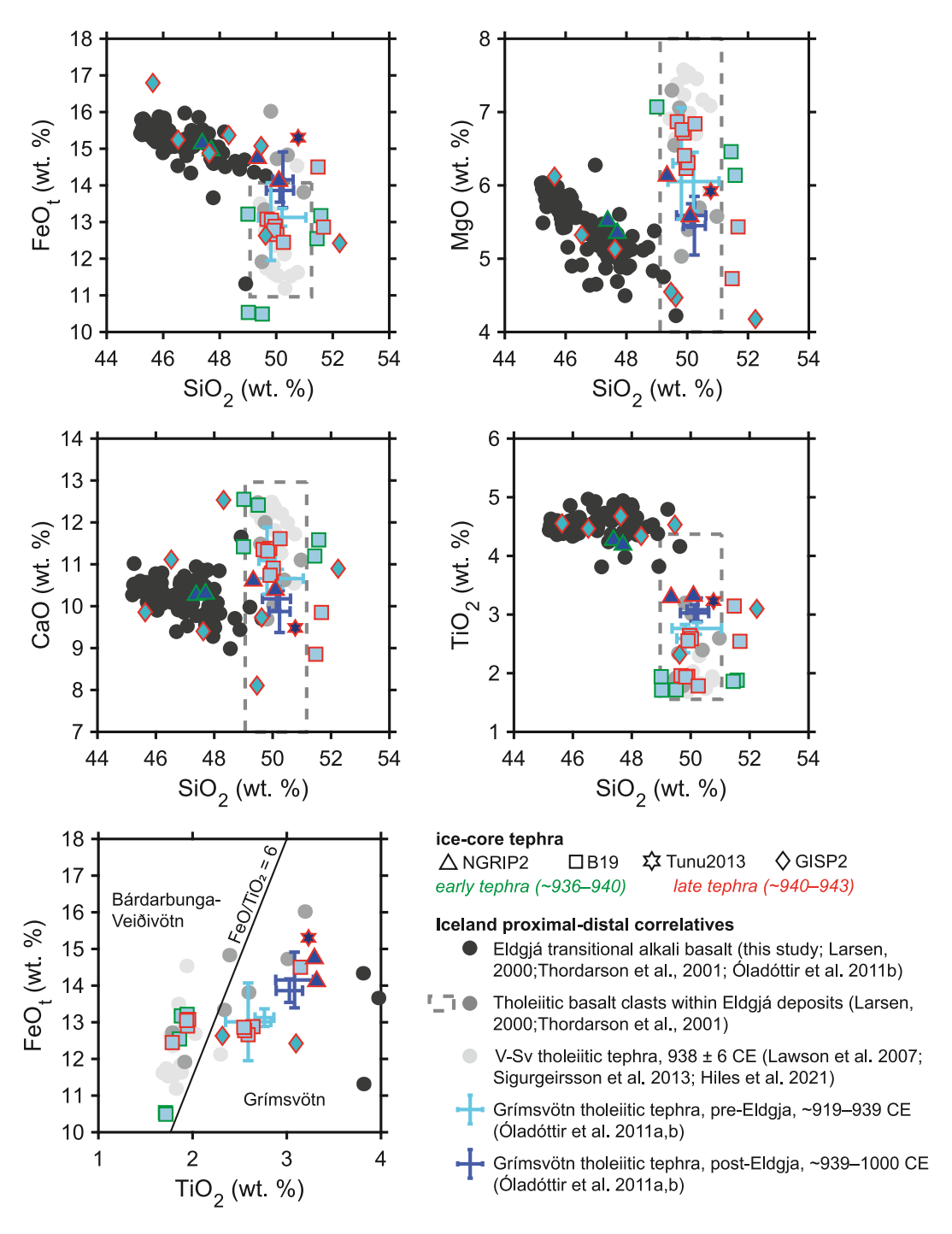


**Figure 6.** Major element Harker diagrams comparing mafic glass found in the ice-core (colored symbols) with Icelandic correlatives (greyscale symbols). Note that for tholeitic basalt clasts within Eldgjá reported by Thordarson et al. (2001) we show the range of values by the gray dashed box. Error bars give the maximum uncertainty in our samples (based on the 2 s.d. values of the closest matrix matched secondary standards).

In Figure 7 we compare the silicic ice-core tephra with available European and North American records. Four populations are identified, these include three distinct groups of rhyolites (in DYE-3, in Tunu2013, and in both NEEM-2011-S1 and NGRIP2) and a cluster of dacite shards found in GISP2 and Tunu2013. The most compelling geochemical match is for rhyolitic tephra found in Tunu2013 between 940 and 942 CE with the Jala Pumice from Volcan Ceboruco in Mexico (Gardner & Tait, 2000). Our compilation also shows good overlap between the

HUTCHISON ET AL. 11 of 21

2169896, 2024, 16, Downloaded from https://agupub.son/inelibrary.wiley.com/doi/10.1029/2023JD040142, Wiley Online Library on [22/082024]. See the Terms and Conditions (https://onlinelibrary.wiley.com/terms-and-conditions) on Wiley Online Library for rules of use; OA articles are governed by the applicable Creative Commons Licensen

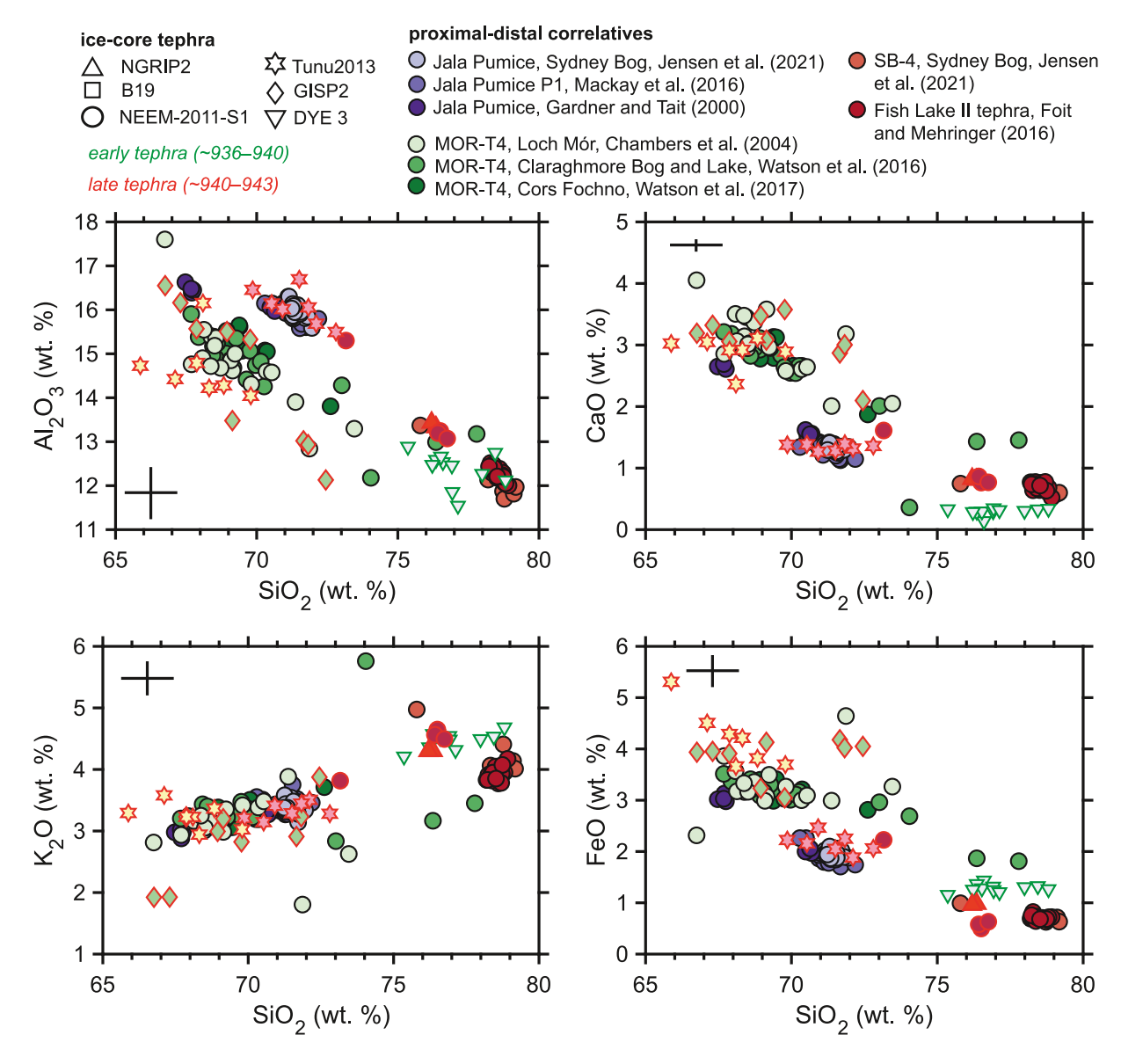


Figure 7. Major element Harker diagrams comparing silicic glass found in the ice-core with proximal-distal correlatives. Error bars give the maximum uncertainty in our samples (based on the 2 s.d. values of the closest matrix matched secondary standards).

dacitic populations in Tunu2013 and GISP2 and the European MOR-T4 tephra, which are roughly contemporaneous with the Eldgjá fissure eruption, and the Jala Pumice (Table 1, Plunkett et al., 2023).

#### 4. Discussion

#### 4.1. Icelandic Volcanic Emissions and Atmospheric Transport

Our network of ice-cores with highly time-resolved records of S, Cl, metals, and particles reveals a complex record of Northern Hemisphere volcanism between 936 and 943 CE. Although geochemical analyses identify several populations of cryptotephra (detailed in Section 4.2) multiple lines of evidence suggest Icelandic emissions are the main volatile and metal contributor. First, tephra matching Eldgjá's transitional alkali basalt chemistry are represented (Figure 6), as are numerous tholeitic shards which can be linked to the nearby Grímsvötn and Bárðarbunga-Veiðivötn systems (Figure 1b). Second, the 936–941 CE S isotope sub-samples (Figure 4) demonstrate above-background S concentrations and  $\delta^{34}$ S values consistent with enhanced volcanic emissions. The measured and background-corrected  $\delta^{34}$ S (-0.5% and -3.9%, respectively) are also much lower

HUTCHISON ET AL. 12 of 21

than  $\delta^{34}S$  values characteristic of arc volcanoes (for which  $\delta^{34}S$  in SO<sub>2</sub> gas and sulfate is usually elevated, ~2‰-10‰, due to high- $\delta^{34}S$  slab input and oxidizing magmas; Martin et al., 2014). Icelandic and rift-related basaltic magmas from Eastern Africa are typically more reduced and display lower  $\delta^{34}S$  (~0‰ to -5‰, cf. compilation of Jongebloed et al., 2023) comparable to the values we observe in the ice-cores (Figure 4). Finally, the  $\Delta^{33}S$  of ice-core sulfate is ~0‰ for most samples indicating that the volcanic S was transported in the upper troposphere or lower stratosphere and requiring an extratropical Northern Hemisphere source (Burke et al., 2019). These data provide valuable new constraints on aerosol transport and are consistent with S emissions from Eldgjá which are sourced from lava fountaining and major explosive phases. The latter are estimated to have fed plumes to heights of ~11–18 km, that is, the lower stratosphere (discussed further in Section 4.3, W. Moreland, 2017).

Further evidence for Icelandic origin is the high concentration of trace metals (Figures 2 and 3). Cd is a volatile metal emitted during volcanic eruptions and is transported and deposited as soluble chloride aerosols (hence its coincidence with peaks in Cl, Mason et al., 2022). Basaltic eruptions emit large quantities of volatile metals (Ilyinskaya et al., 2017), and in Greenland ice-cores, Cd peaks of this magnitude have been observed only for Icelandic fissure eruptions (e.g., the 1783 Laki eruption: Wei et al., 2008) and not mid- to high-latitude arc eruptions (e.g., the VEI 6 1912 Katmai/Novarupta or 852/3 CE Mount Churchill eruptions, Mackay et al., 2022). Thus, the co-located Cl and Cd peaks (Figures 2 and 3) strongly support a volcanic emission from a relatively close source region, that is, the basaltic fissure eruptions in Iceland.

Comparing inland and coastal cores provides further insights into volcanic emissions and plume processes. One of the most striking features is that while peak nssCl and nssS concentrations are roughly equivalent at inland sites (Figure 2), at RECAP (the nearest to Iceland, Figure 1a), nssCl dominates the volcanic fallout (Figure 3). HCl is highly soluble and hence when liquid water is more abundant (i.e., in the troposphere) it is likely to be rapidly scavenged from the volcanic plume (Halmer et al., 2002; Textor et al., 2003). Coastal sites like RECAP are heavily influenced by maritime conditions and experience greater precipitation (wet deposition) than inland sites (Bromwich et al., 1999). Thus, the exceptionally high concentrations of nssCl at RECAP most likely reflect its relative proximity to the fissure source, and the fact that Cl species are washed out faster in the moister, lower altitudes of plume transport captured at coastal sites.

All inland sites show prominent Cd and Cl peaks (Figure 2) ~6 months after the mid-939 CE S peak. This could be explained by processes at source (i.e., changes in eruption chemistry and/or style) or changing transport and chemical evolution of the plume. Changes in eruption style from phreatomagmatic to magmatic eruptions are well documented for Eldgjá and have been linked to transitions from subglacial to subaerial fissures (W. M. Moreland et al., 2019). Magma-water interaction during subglacial phases is expected to more efficiently scavenge S and particularly Cl from the plume (given the high solubility of HCl). Thus, the later Cd and Cl peak might represent a transition from subglacial (phreatomagmatic) to subaerial (magmatic) eruptions and a reduction in volatile scrubbing. Alternatively, the changing deposition could reflect changes in synoptic meteorology and plume dispersal. Prevailing winds in Iceland vary seasonally (Einarsson, 1984) and a key observation from recent fissure eruptions (i.e., 2014–2015 Holuhraun eruption, Ilyinskaya et al., 2017) is that metal concentrations in the plume rapidly decline (by several orders of magnitude) within a few 100 km of the vent. In the case of Eldgjá, the initial mid-939 CE S peak could represent a mature plume that had circled the Arctic basin and deposited its Cl and metals before arriving in Greenland. The later Cd- and Cl-rich S peak might then reflect direct transport of emissions toward Greenland resulting in deposition from a less atmospherically-processed plume to the ice sheet. Isopach maps are available for the first 11 (out of 16) eruptive units (W. M. Moreland et al., 2019) and show that ash was dispersed predominantly toward the south-east. This lends some support to the second hypothesis and leaves open the possibility that there was a change in plume dispersal during the final eruptive phases. Without tighter constraints on synoptic weather and tephra dispersal for the latter phases we cannot discriminate between these scenarios, though this aspect could be explored through volcanic plume modeling.

Although transitional alkali basalt shards that match the main Eldgjá products occur in 939/940 CE (Figure 6, Section 4.2), Icelandic volcanism in the years prior to 939 CE is expected from proximal records (Table 1) and signaled in several ice-core data sets. These include CFA records which show increasing S deposition in Tunu2013 and B19 beginning in 936 CE (Figure 2), and our cryptotephra investigations which identified tholeitic basaltic glass with Bárðarbunga-Veiðivötn chemistries in B19 at around 936/937 CE (Figure 5b). More subtle S peaks are observed in NEEM-2011-S1 and NGRIP2, but for the latter, S isotopes (Figure 4) clearly support an

HUTCHISON ET AL. 13 of 21

enhanced volcanic flux via the upper troposphere/lower stratosphere and hence a relatively close source, most likely Icelandic, throughout 936–939 CE.

A key question is: which Icelandic volcanic system is responsible for the S emissions through 936–939 CE? The only Icelandic cryptotephra are those in B19 in 936/937 CE which match the Bárðarbunga-Veiðivötn system (Figure 5b), and so one possibility is that this fissure continued to be active until Eldgjá in 939 CE. Another potential source for the S emissions could be Grímsvötn, which is known to have been active a few years before Eldgjá (Table 1, Óladóttir, Larsen, & Sigmarsson, 2011). A further possibility is that there were some early explosive phases of the Eldgjá fissure which occurred before the major eruption in 939 CE and contributed to the volcanic S deposition. Unfortunately, with no basaltic cryptotephra from late 937 to mid-939 CE period we cannot distinguish which scenario is most likely. Nevertheless, by 939 CE the Eldgjá fissure eruption was underway, and the large quantities of S, Cl, and metals reaching Greenland suggest that by the end of 939 CE the eruption was predominantly sub-aerial, allowing these reactive species to remain in the airborne plume.

In summary, our new high-resolution ice-core records highlight a sustained (~4 year) period of S emissions and episodic ash emissions from three different volcanic systems: Bárðarbunga-Veiðivötn, Grímsvötn, and Eldgjá (which belongs to the Katla volcanic system, Figure 1). We identify changes in volatile deposition which likely reflect changing eruption style at Eldgjá and transitions between phreatomagmatic and magmatic phases. These corroborate many of the interpretations of proximal records made by Thordarson et al. (2001), Óladóttir, Larsen, and Sigmarsson (2011), and W. M. Moreland et al. (2019), and significantly improve our understanding of this major spatio-temporal clustering of volcanism in southern Iceland.

#### 4.2. New Insights From Cryptotephra Records

Here we discuss the Icelandic tephra record and cryptotephra linkages across the Atlantic. In Iceland, several basaltic tephra layers and chemistries are found and dated to early- to mid-10th century (Table 1). Within the Eldgjá tephra deposits, Thordarson et al. (2001) found evidence for several juvenile tephra products. Although transitional alkali basalt dominates the tephra deposits, tholeiitic basalt is found as clasts throughout, and while it was volumetrically minor (<5%) at most localities, in the northernmost section of the fissure tholeiitic clasts were the most abundant type. Tholeiitic clasts in the Eldgjá deposits have a range of compositions with both Bárdarbunga-Veiðivötn and Grímsvötn affinities (Figure 6). Evidence for roughly contemporaneous eruptions of Grímsvötn have been found in soil sections around the Vatnajökull ice-cap by Óladóttir, Larsen, and Sigmarsson (2011) who identified tholeiitic Grímsvötn tephra pre- and post-dating Eldgjá (Table 1). Evidence for Bárdarbunga-Veiðivötn eruptions during this period are well-documented in the north of Iceland, where the tephra record is dominated by the tholeiitic basalt V-Sv with an age 938 ± 6 CE (Schmid et al., 2017; Sigurgeirsson et al., 2013). The eruptive vent for V-Sv is not identified but its chemistry provides a firm link to Bárdarbunga-Veiðivötn (Sigurgeirsson et al., 2013; Figure 6). We are unaware of any sites where both the Eldgjá and V-Sv tephras are found, and it remains unclear whether V-Sv pre- or post-dates Eldgjá.

A key result of our cryptotephra investigation is the identification of transitional alkali basalt shards in NGRIP2 and GISP2 (Figure 6). These provide the first robust EPMA match between the ice-core tephra record and the main Eldgjá eruptive products and confirm eruption of Eldgjá in 939–940 CE. However, as outlined in Section 4.1, an important caveat is that volcanic S emissions are elevated above background through 936–939 CE and do leave open the possibility of eruptive activity at Eldgjá or other Icelandic fissure systems prior to 939 CE. As noted in Section 4.1 we also found a wide variety of tholeiitic basalt shards throughout our ice-core record. Bárdarbunga-Veiðivötn compositions are observed in B19 in 936/937 CE and 940–941 CE, while Grímsvötn compositions are observed through 940–942 CE (in NGRIP2, Tunu2013 and GISP2, Figures 5 and 6). Even with the high time resolution (~2-month) sampling in GISP2 we still found tholeiitic basalt tephra (with Grímsvötn composition) alongside transitional alkali basalt tephra, precluding resolution of their time sequence. If surprising, this is nevertheless consistent with the Eldgjá deposit stratigraphy of Thordarson et al. (2001), who found various tholeiitic clasts throughout the proximal transitional alkali basalt sequence.

V-Sv tephra have a typical Bárdarbunga-Veiðivötn composition (Figure 6) and while various ice-core shards overlap the chemistry of V-Sv the closest match on all elements appears to be with the late tephra shards from B19 (with an age of 940–941 CE). Several tholeiitic clasts sampled within the Eldgjá tephra deposits by Thordarson et al. (2001) also show compositions akin to V-Sv and to explain these observations we require a single V-Sv eruption, or multiple Bárdarbunga-Veiðivötn eruptions with very similar chemistry. Given the overlapping

HUTCHISON ET AL. 14 of 21

ages of V-Sv (938  $\pm$  6 CE, Sigurgeirsson et al., 2013; Schmid et al., 2017) and Eldgjá (939–40 CE, Oppenheimer et al., 2018, this study), we tentatively correlate this B19 tephra with V-Sv (yielding an age of 940–941 CE for this eruption). We emphasize though that as the numbers of V-Sv matching shards in both the ice-core and the Eldgjá tephra deposits are small, further work would be necessary to test this hypothesis (as outlined below).

An additional correlation can be made between Grímsvötn tephra known to post-date Eldgjá (Óladóttir, Larsen, & Sigmarsson, 2011), and the late NGRIP2 tephra (Figure 6). Again, this geochemical match is proposed with caution as it is based on a handful of glass shard analyses from both ice-core and proximal deposits, but it is consistent with available information on timing (Table 1) and chemistry (Figure 6). Clearly, the limited number of tholeiitic shards and their chemical similarity (in terms of major elements) makes correlations challenging. Trace element analysis may help to discriminate these geochemical populations, but the small ice-core shard sizes (Figure S2 in Supporting Information S1) challenge the use of laser ablation which typically requires a spot size of >10 μm. Additional field investigations of the northern Eldgjá fissure segment, where tholeiitic tephra appear to be more abundant, might ultimately resolve the relative timing of V-Sv and Eldgjá. Ultimately, our data provide a more nuanced understanding of Icelandic volcanism and precise constraints on eruption timing. These data highlight episodic tholeiitic activity from 936 to 941 CE that can be linked to Bárdarbunga-Veiðivötn and Grímsvötn systems and confirm the main Eldgjá transitional alkali basalt tephra eruption occurred in 939–940 CE.

Our study and previous ice-core cryptotephra research (Coulter et al., 2012; Sun et al., 2014; Zielinski et al., 1995), as well as studies of lake sediment and peatland cores (e.g., Jensen et al., 2021; Mackay et al., 2016; Plunkett & Pilcher, 2018) document numerous silicic eruptions in the  $\sim$ 930–950 CE time period, but to date there are no linkages between Europe, North America, and Greenland. In the Tunu2013 ice-core at  $\sim$ 941 CE we identified numerous shards matching the Jala Pumice from Volcan Ceboruco in Mexico (Gardner & Tait, 2000). The ice-core timing is compatible with radiocarbon ages for the Jala Pumice obtained at Villagedale and Sidney Bog in North America (889–1130 CE and 910–1270 CE, respectively; Mackay et al., 2016; Jensen et al., 2021) and Faddanmore in Ireland ( $\sim$ 937  $\pm$  10 CE; Plunkett & Pilcher, 2018; Plunkett et al., 2023), as well as proximal radiocarbon dates which mostly range between  $\sim$ 890 and  $\sim$ 990 CE (Sieron & Siebe, 2008). This allows us to provide a new and robust date of 941  $\pm$  1 CE for this VEI 6 caldera-forming eruption, and a valuable tie point between Europe, North America, and Greenland. It is notable that between 940 CE and 943 CE all ice-core records show declining S concentrations and subsidiary S peaks (Figure 2). This suggests that the S yield, which has yet to be quantified petrologically for the Jala Pumice eruption, was modest (although stratospheric transport of S is plausibly supported by  $\Delta^{33}$ S, Figure 4c).

Jensen et al. (2021) found that in Sidney Bog (north-eastern North America) another tephra, SB-4, occurs in the same interval as the Jala Pumice. SB-4 is a high-SiO<sub>2</sub> rhyolite (Figure 7), and Jensen et al. (2021) proposed a North American (Cascades) source because it matches the chemistry and timing of an eruption at Lassen volcanic center (Fish Lake II tephra, correlated with the most recent eruption of Chaos Crags; Foit & Mehringer, 2016). In the Tunu2013 ice-core, we also found another silicic tephra in the same sub-sample as Jala (Figure 5), but it has a trachytic-dacitic composition that does not match SB-4 chemistry. There is some resemblance between a rhyolitic tephra reported from the Dye-3 ice-core by Coulter et al. (2012) and SB-4 (Figure 7) but clear offsets in CaO,  $K_2O$ , and FeO (Figure 7) preclude a geochemical match. SB-4 has yet to be identified in contemporary European tephra records and given its apparent absence in Greenland, this would suggest its spatial distribution is limited to North America.

In Europe, MOR-T4 is a key Holocene tephra layer (Chambers et al., 2004; Watson et al., 2016, 2017). Its age is constrained as  $\sim$ 937  $\pm$  10 CE (Plunkett & Pilcher, 2018; Plunkett et al., 2023), and it comprises multiple glass populations including the Jala Pumice (dated to 941  $\pm$  1 CE, above). The sources of the other MOR-T4 shards are unknown but it is worth noting that the main cluster with SiO<sub>2</sub> of 67–70 wt.% (Figure 7) shows a fair correspondence with a number of ice-core shards from Tunu2013 and GISP2. Certainly, for the major elements that are in greatest abundance (i.e., >1 wt.%, Figure 7) numerous shards overlap with or are within error of the MOR-T4 population. This correlation allows us to establish an age range of 940–941 CE for MOR-T4, and its coincidence with the Jala Pumice reinforces the point that MOR-T4, and by extension other Holocene tephra layers in sedimentary sequences, may represent multiple eruptive events.

HUTCHISON ET AL. 15 of 21

21698996, 2024, 16, Downloaded from https://agupubs.

onlinelibrary.wiley.com/doi/10.1029/2023JD040142, Wiley Online Library on [22/08/2024]. See the Terms and Conditions

The new ice-core data provide a wealth of insights into volcanism around 936–943 CE (summarized in Figure 8). Icelandic eruptions appear to have initiated around 936/937 CE and continued until 940/941 CE. Proximal and distal records confirm multiple magmas erupted during this period (Section 4.2; Óladóttir, Larsen, & Sigmarsson, 2011; Schmid et al., 2017; Sigurgeirsson et al., 2013; Thordarson et al., 2001), and high time resolution cryptotephra sub-sampling (Figure 5, GISP2) and CFA (Figure 2, B19 and Tunu2013) confirms several episodes of explosive eruptions. All cores show major S, Cl, and volatile metal deposition in 939 CE and we hypothesize that the transition from low volcanic S deposition in 936–938 CE to high volcanic S deposition in 939 CE reflects a general shift from low magnitude eruptions, initially associated with the Bárðarbunga-Veiðivötn and/or Grímsvötn eruptions (and possibly, some early phreatomagmatic episodes of Eldgjá), to the high magnitude explosive and effusive episodes of Eldgjá.

Climate conditions during the period of study can be evaluated via tree-ring temperature reconstructions (Figure 8). Northern Hemisphere May-August (MJJA) temperature anomalies relative to the 926–935 CE pre-eruption mean from Wilson et al. (2016), Anchukaitis et al. (2017), Stoffel et al. (2015), and Schneider et al. (2015) all identify a marked cooling of 0.4–0.9°C in the summer of 940 CE and recovery the following year. Several records (i.e., SCH15, stNH1, and ANCH17 in Figure 8) suggest minor cooling starting around 937/938 CE. However, these signals do not exceed interannual variability evident in these reconstructions (i.e., there is no evidence of significant cooling prior to 940 CE).

Stothers (1998) and Oppenheimer et al. (2018) examined possible consequences of climate forcing arising from the Eldgjá eruption; these include documentary evidence of atmospheric optical phenomena (i.e., haze in 939 CE), severe winters (939/940, 940/941, and 941/942 CE in Europe and China) and food crises (939–942 CE in Europe, China, and the Middle East). It is notable that our non-zero  $\Delta^{33}$ S values which show a muted positive to negative variation (Figure 4) indicative of stratospheric aerosol, occur in 940 CE and 941 CE, coincident with summer cooling and severe winters in the Northern Hemisphere (Figure 8). This observation strongly supports volcanic S emissions as the cause of the apparent cooling. However, our cryptotephra records demonstrate that Eldgjá was not the only eruption at this time, and while the observations of haze in Europe are consistent with the Eldgjá fissure eruption, attribution of these climatic and societal impacts to Eldgjá is complicated by four coincident eruptions (Figure 8). Our new discovery of the VEI 6 Jala Pumice at 941  $\pm$  1 CE suggests that these unknown eruptions may be of considerable magnitude, but since their S emissions remain unknown, Eldgjá, with its exceptional (185 Tg) SO<sub>2</sub> emission to upper tropospheric/lower stratospheric altitudes (Thordarson et al., 2001), remains the prime candidate for any climate cooling.

Further evidence that climate cooling is linked to Eldgjá S emissions are the muted positive to negative  $\Delta^{33}$ S signal that occurs over a short (~1 year) duration. This is very different to the 2–3 year long signature of low latitude eruptions associated with stratospheric aerosol veils (e.g., Pinatubo and Tambora; Baroni et al., 2007; Burke et al., 2019). This indicates a short atmospheric residence time for the 940–941 CE stratospheric veil and supports an extratropical Northern Hemisphere source. Consistent with this is the abrupt, 1-year summer cooling signature in the tree-ring reconstructions, which contrasts with the multiyear cooling signals usually associated with major low-latitude sulfur-rich explosive eruptions (Sigl et al., 2015; Stoffel et al., 2015). This too supports a short residence time for the stratospheric aerosol consistent with a mid- to high- latitude source, and given the 940 CE Cl and volatile metal peaks are clear indications of Icelandic volcanism (Section 4.1) Eldgiá provides the most viable source. Plume injection height is also a key parameter controlling the radiative forcing of volcanic aerosols and as discussed in Section 4.1 the  $\sim 0\%$   $\Delta^{33}$ S of the main 939 CE S peak evidences upper tropospheric and/or lower stratospheric injection and agrees with the ~11-18 km eruption column heights estimated for magmatic and phreatomagmatic phases of Eldgjá by W. Moreland (2017). Lower stratospheric S injections can still result in significant radiative forcing and hence surface cooling (e.g., Fuglestvedt et al., 2024; Krishnamohan et al., 2019), and we reiterate that multiple lines of evidence point to Eldgjá as the strongest contender for volcanic climate cooling.

Another notable feature of the ice-cores is the large Na peaks in winter 939/940 CE. These are particularly pronounced in coastal sites and are well above typical background values from the first millennium of the Common Era (Figure S1 in Supporting Information S1). Chemical transport models of Rhodes et al. (2018) show that Na in coastal ice-cores is primarily sourced from the sea ice surface, and thus this remarkable increase in sea ice aerosol contributions suggests a large increase in sea ice extent. The fact that Na peaks closely follow the

HUTCHISON ET AL. 16 of 21

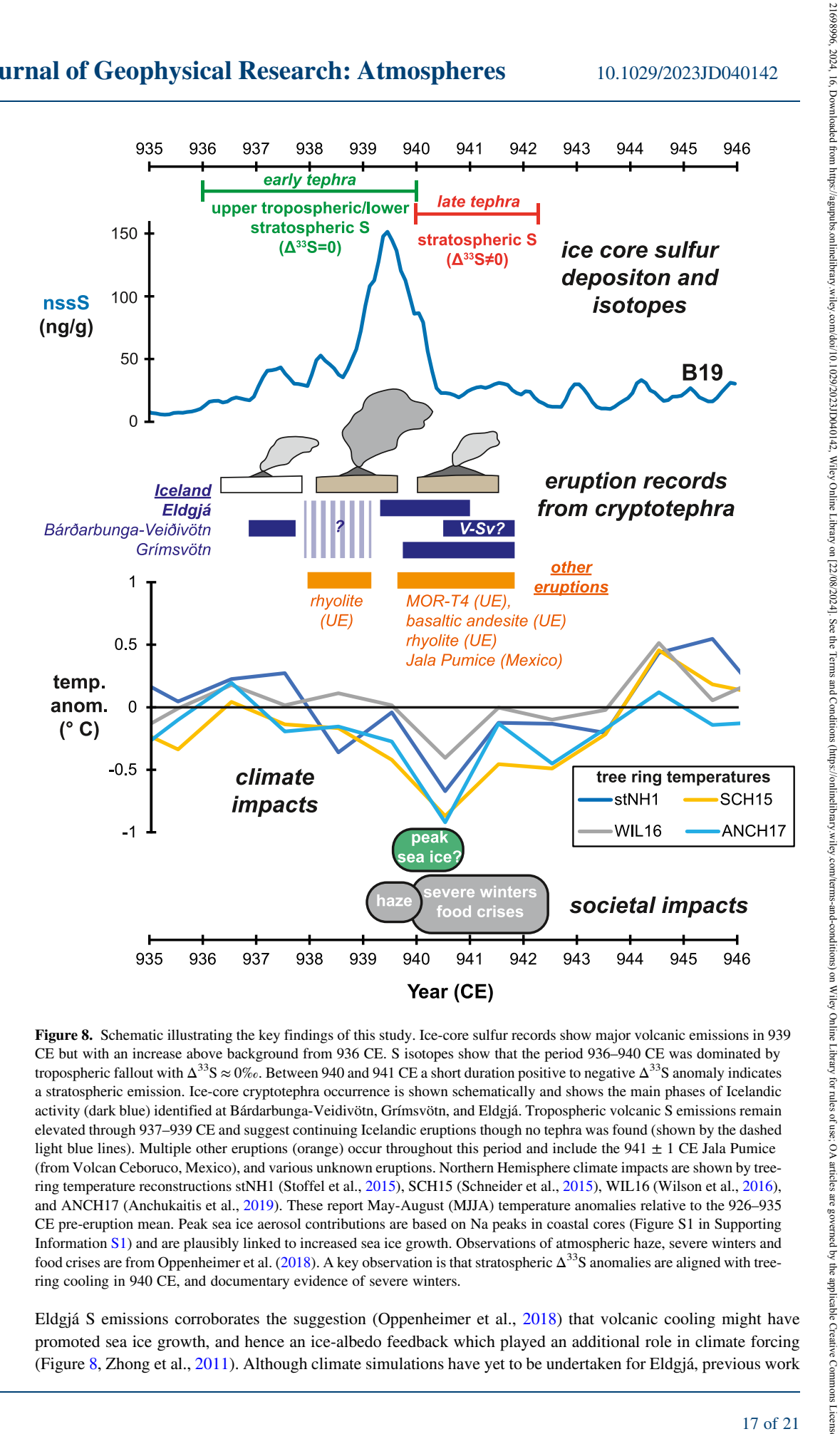


Figure 8. Schematic illustrating the key findings of this study. Ice-core sulfur records show major volcanic emissions in 939 CE but with an increase above background from 936 CE. S isotopes show that the period 936-940 CE was dominated by tropospheric fallout with  $\Delta^{33}$ S  $\approx 0\%$ . Between 940 and 941 CE a short duration positive to negative  $\Delta^{33}$ S anomaly indicates a stratospheric emission. Ice-core cryptotephra occurrence is shown schematically and shows the main phases of Icelandic activity (dark blue) identified at Bárdarbunga-Veidivötn, Grímsvötn, and Eldgjá. Tropospheric volcanic S emissions remain elevated through 937-939 CE and suggest continuing Icelandic eruptions though no tephra was found (shown by the dashed light blue lines). Multiple other eruptions (orange) occur throughout this period and include the 941 ± 1 CE Jala Pumice (from Volcan Ceboruco, Mexico), and various unknown eruptions. Northern Hemisphere climate impacts are shown by treering temperature reconstructions stNH1 (Stoffel et al., 2015), SCH15 (Schneider et al., 2015), WIL16 (Wilson et al., 2016), and ANCH17 (Anchukaitis et al., 2019). These report May-August (MJJA) temperature anomalies relative to the 926-935 CE pre-eruption mean. Peak sea ice aerosol contributions are based on Na peaks in coastal cores (Figure S1 in Supporting Information \$1) and are plausibly linked to increased sea ice growth. Observations of atmospheric haze, severe winters and food crises are from Oppenheimer et al. (2018). A key observation is that stratospheric  $\Delta^{33}$ S anomalies are aligned with treering cooling in 940 CE, and documentary evidence of severe winters.

Eldgiá S emissions corroborates the suggestion (Oppenheimer et al., 2018) that volcanic cooling might have promoted sea ice growth, and hence an ice-albedo feedback which played an additional role in climate forcing (Figure 8, Zhong et al., 2011). Although climate simulations have yet to be undertaken for Eldgjá, previous work

HUTCHISON ET AL. 17 of 21

21698996, 2024, 16, Downloaded from https://agupubs.onlinelibrary.wiley.com/doi/10.1029/2023JD040142, Wiley Online Library on [22/08/2024]. See the Terms and Conditions (https://onlinelibrary.wiley.com/terms/

of van Dijk et al. (2022) showed that large northern Hemisphere extratropical eruptions can generate a significant sea ice increase over a period of ~0–3 years after eruption. Given Eldgjá's relatively high latitude and its large emission of upper tropospheric/lower stratospheric S, a similar short-term sea ice response seems plausible and is supported by the peak values of coastal Na in 939–940 CE. Clearly, climate simulations of an Eldgjá eruption scenario would be extremely enlightening for evaluating radiative forcing and the potential role of sea ice feedbacks.

Much of our understanding of the timescales and impacts of Icelandic fissure eruptions is based on the 1783 Laki eruption (Thordarson & Self, 2003), and it is interesting to compare these two Icelandic fissure eruptions (Morison et al., 2024). Ice-core and proximal records reveal a cluster of Icelandic fissure eruptions from at least three sources (Bárðarbunga-Veiðivötn, Grímsvötn and Eldgjá) in 936-941 CE which contrast with the homogenous quartz-tholeiite magma erupted at Laki (Guilbaud et al., 2007). Eldgjá appears to be significantly larger than Laki: first, the length of Eldgiá fissure (75 km) is roughly three times that of Laki (27 km), and second, the estimated eruptive volumes of lavas and tephra were greater (19.7 vs. 14.7 and 1.3 vs. 0.4 km<sup>3</sup>, for Eldgjá and Laki respectively). The overall duration of Eldgjá is constrained by our cryptotephra to at least to 939-940 CE (Section 4.2) and is much longer than Laki (~2 years vs. 8 months) though we note that both eruptions involved multiple pulses. Petrological estimates of SO<sub>2</sub> emissions, which rely in part on estimated eruptive volumes, suggest a larger mass of SO<sub>2</sub> was injected to upper tropospheric and lower stratospheric heights by Eldgjá (185 Tg, compared to 122 Tg for Laki, Thordarson & Self, 2003; Thordarson et al., 2001). Despite these differences, averaged ice-core sulfate deposition in Greenland is somewhat lower for Eldgjá although still within uncertainty (Eldgjá =  $89 \pm 23 \text{ kg km}^{-2}$  and Laki =  $136 \pm 36 \text{ kg km}^{-2}$ , Sigl et al., 2015). This suggests that a greater proportion of Laki S reached Greenland, and this might reflect the fact that phreatomagmatic activity, and hence S scrubbing, was much more limited at Laki because it was mainly a subaerial fissure (Thordarson & Self, 1993). Eldgjá, by contrast, is represented by significant subglacial fissure segments and major phreatomagmatic units (W. M. Moreland et al., 2019). For both Laki and Eldgjá severe winters follow the main S emission, suggesting these large basaltic fissure events may be responsible for abrupt climate cooling (Zambri et al., 2019). For Eldgiá the story is complicated by coincident eruptions (Section 4.2), and a next step will be to simulate an Eldgjá-only scenario and explore different eruption pulses and their response in climate models.

#### 5. Conclusions

We generated new high-resolution ice-core records to improve understanding of the timing, duration, and impacts of global volcanism in the 936–943 CE period, with a particular interest in Icelandic fissure eruptions. These records show Icelandic eruptions initiated in 936/937 CE, with major S, Cl, and volatile metal emission and deposition occurring in 939 CE, and continued episodic ash emissions until 940/941 CE. Our new records confirm a major eruption of Eldgjá to 939–940 CE and also reveal enhanced volcanic emissions through 936–941 CE linked to three fissure systems (Grímsvötn, Bárðarbunga-Veiðivötn and Eldgjá). We also identify a potential correlative of V-Sv tephra from the Bárðarbunga-Veiðivötn system at 940–941 CE.  $\Delta^{33}$ S values measured in ice-cores across the 936–941 CE period show that S was mainly transported at upper tropospheric or lower stratosphere altitudes consistent with these Icelandic fissure sources. Importantly, at least four silicic tephra populations are represented in this period. One of these we attribute to the Jala Pumice from Volcan Ceboruco (Mexico), and our new ice-core discovery provides a precise date of 941  $\pm$  1 CE for this VEI 6 caldera-forming event, and a valuable tephrostratigraphic linkage between North America, Greenland, and Europe.

Northern Hemisphere summer cooling of  $0.4\text{--}0.9^{\circ}\text{C}$  in 940 CE is consistent with the timing of a short-lived stratospheric sulfate aerosol veil (based on anomalous ice-core  $\Delta^{33}\text{S}$ ). However, our cryptotephra populations evidence a cluster of eruptions at this time. While Eldgjá remains a prime candidate owing to the estimated magnitude of  $\text{SO}_2$  emission, the extent to which it is implicated in climate and societal impacts is uncertain. Our study reveals a more nuanced picture of volcanism between 936 and 943 CE. It reveals a significant spatiotemporal clustering of volcanism in south Iceland and highlights the challenges of disentangling the contributions of multiple eruptions to atmospheric and climatic change.

HUTCHISON ET AL. 18 of 21



### Journal of Geophysical Research: Atmospheres

10.1029/2023JD040142

#### **Data Availability Statement**

The research data underpinning this publication can be accessed at https://doi.org/10.17630/cbc85cdf-6a90-4923a53b-c2e9cd02dfab. All data is available in Supporting Information, tables, and/or figures. Data produced during this study are also provided in Data Set S1-S3.

Acknowledgments W. Hutchison is funded by a UKRI Future Leaders Fellowship (MR/S033505/1). I. Gabriel and M. Sigl are supported by the European Research Council Grant under the European Union's Horizon 2020 research and innovation program (820047), I. Gabriel received funding from the Swiss Polar Institute and BNP Paribas Swiss Foundation, A. Burke is supported by a Leverhulme Trust Prize (PLP-2021-167). The St Andrews EPMA was supported by the EPSRC Light Element Analysis Facility Grant EP/T019298/1 and the EPSRC Strategic Equipment Resource Grant EP/R023751/1. K. Krüger and M. Sigl acknowledge funding for this study by the Research Council of Norway/ University of Oslo Toppforsk project "VIKINGS" with the Grant 275191. R. Wilson is supported by the Natural Environment Research Council project Vol-Clim (NE/S000887/1). Ongoing development of the DRI Arctic array of continuous ice-core glaciochemical records was supported by NSF and other grants to J.R. McConnell. These included Grants 1204176 and 0909541 for collection and continuous analyses of the Tunu2013 and NEEM-2011-S1 cores. respectively, as well as Grants 1925417, 1204176, and 1023672 for analyses of the RECAP, B19, and Flade Isblink archived cores, respectively. The John Fell Oxford University Press (OUP) Research Fund and All Souls College, Oxford, as well as the DRI, supported analysis and interpretation of archived NGRIP2 icecore samples. We thank the NGRIP, NEEM, RECAP, North Greenland Traverse, Flade Isblink, and other science consortia for providing ice-core samples and field support, and the students and staff in the DRI ice-core laboratory for their assistance. We acknowledge support from the GISP2 community; M. Twickler, and the NSF-ICF for providing access to archived Tunu2013 and GISP2 samples; J. P. Steffensen, A. Svensson, I. Koldtoft from the Niels Bohr for access to NGRIP2 samples. We thank C. Brashear and P. Abbott for their assistance in sampling icecores. We thank T. Thordarson, B. Óladóttir, S. Ferrandin and H.F. Fuglestvedt for their support and discussions during field-campaigns in Iceland. We thank P. Lanari and P. Abbott for assistance during Bern EPMA analyses. This work benefited from participation by several authors in the Past Global Changes Volcanic Impacts on Climate and Society working group. Finally, we thank Yongyun Hu for editorial handling and three anonymous reviewers for their detailed and constructive

comments.

#### References

- Anchukaitis, K. J., Cook, E. R., Cook, B. I., Pearl, J., D'Arrigo, R., & Wilson, R. (2019). Coupled modes of North Atlantic Oceanatmosphere variability and the onset of the little ice age. Geophysical Research Letters, 46(21), 12417-12426. https://doi.org/10.
- Anchukaitis, K. J., Wilson, R., Briffa, K. R., Büntgen, U., Cook, E. R., D'Arrigo, R., et al. (2017). Last millennium northern hemisphere summer temperatures from tree rings: Part II, spatially resolved reconstructions. Quaternary Science Reviews, 163, 1–22. https://doi.org/10.1016/j. quascirev.2017.02.020
- Baroni, M., Thiemens, M. H., Delmas, R. J., & Savarino, J. (2007). Mass-independent sulfur isotopic compositions in stratospheric volcanic eruptions. Science, 315(5808), 84-87. https://doi.org/10.1126/science.1131754
- Bromwich, D. H., Chen, Q. S., Li, Y., & Cullather, R. I. (1999). Precipitation over greenland and its relation to the north Atlantic Oscillation. Journal of Geophysical Research, 104(D18), 22103-22115. https://doi.org/10.1029/1999JD900373
- Burke, A., Moore, K. A., Sigl, M., Nita, D. C., McConnell, J. R., & Adkins, J. F. (2019). Stratospheric eruptions from tropical and extra-tropical volcanoes constrained using high-resolution sulfur isotopes in ice cores. Earth and Planetary Science Letters, 521, 113-119. https://doi.org/10. 1016/j.epsl.2019.06.006
- Burke, A., Present, T. M., Paris, G., Rae, E. C. M., Sandilands, B. H., Gaillardet, J., et al. (2018). Sulfur isotopes in rivers: Insights into global weathering budgets, pyrite oxidation, and the modern sulfur cycle. Earth and Planetary Science Letters, 496, 168-177. https://doi.org/10.1016/
- Cerling, T. E., Brown, F. H., & Bowman, J. R. (1985). Low-temperature alteration of volcanic glass: Hydration, Na, K, 18O and Ar mobility. Chemical Geology: Isotope Geoscience section, 52(3-4), 281-293. https://doi.org/10.1016/0168-9622(85)90040-5
- Chambers, F. M., Daniell, J. R. G., Hunt, J. B., Molloy, K., & O'Connell, M. (2004). Tephrostratigraphy of an Loch Mór, Inis Oírr, Western Ireland: Implications for Holocene tephrochronology in the northeastern Atlantic region. The Holocene, 14(5), 703-720. https://doi.org/10. 1191/0959683604h1749rp
- Clynne, M. A., Christiansen, R. L., Trimble, D. A., & McGeehin, J. P. (2008), Radiocarbon dates from volcanic deposits of the Chaos Crags and Cinder Cone eruptive sequences and other deposits, Lassen volcanic National Park and vicinity, California. In US Geological Society open-file report, California, USA (Vol. 02-290).
- Coulter, S. E., Pilcher, J. R., Plunkett, G., Baillie, M., Hall, V. A., Steffensen, J. P., et al. (2012). Holocene tephras highlight complexity of volcanic signals in Greenland ice cores. Journal of Geophysical Research, 117(21), D21303. https://doi.org/10.1029/2012JD017698
- Crick, L., Burke, A., Hutchison, W., Kohno, M., Moore, K. A., Savarino, J., et al. (2021). New insights into the ~74 ka Toba eruption from sulfur isotopes of polar ice cores. Climate of the Past, 17(5), 2119-2137. https://doi.org/10.5194/cp-17-2119-2021
- Einarsson, M. Á. (1984). Climate of Iceland. World Survey of Climatology, 15(110), 673-697.
- Foit, F. F., & Mehringer, P. J. (2016). Holocene tephra stratigraphy in four lakes in southeastern Oregon and northwestern Nevada, USA. Quaternary Research, 85(2), 218-226. https://doi.org/10.1016/j.yqres.2015.12.008
- Fuglestvedt, H. F., Zhuo, Z., Toohey, M., & Krüger, K. (2024). Volcanic forcing of high-latitude Northern Hemisphere eruptions. Npj Climate and Atmospheric Science, 7(1), 1-12. https://doi.org/10.1038/s41612-023-00539-4
- Gabriel, I., Plunkett, G., Abbott, P. M., Behrens, M., Burke, A., Chellman, N., et al. (2024). Decadal-to-centennial increases of volcanic aerosols from Iceland challenge the concept of a Medieval Quiet Period. Communications Earth and Environment, 5(1), 194. https://doi.org/10.1038/ s43247-024-01350-6
- Gardner, J. E., & Tait, S. (2000). The caldera-forming eruption of Volcán Ceboruco, Mexico. Bulletin of Volcanology, 62(1), 20–33. https://doi.
- Gautier, E., Savarino, J., Erbland, J., & Farquhar, J. (2018). SO2 oxidation Kinetics leave a consistent isotopic Imprint on volcanic ice core sulfate. Journal of Geophysical Research: Atmospheres, 123(17), 9801-9812. https://doi.org/10.1029/2018JD028456
- Gautier, E., Savarino, J., Hoek, J., Erbland, J., Caillon, N., Hattori, S., et al. (2019). 2600-years of stratospheric volcanism through sulfate isotopes.  ${\it Nature~Communications,~10} (1),~1-7.~https://doi.org/10.1038/s41467-019-08357-0$
- Guilbaud, M.-N., Blake, S., Thordarson, T., & Self, S. (2007). Role of Syn-eruptive cooling and degassing on textures of lavas from the ad 1783-1784 Laki eruption, south Iceland. Journal of Petrology, 48(7), 1265-1294. https://doi.org/10.1093/petrology/egm017
- Halmer, M. M., Schmincke, H. U., & Graf, H. F. (2002). The annual volcanic gas input into the atmosphere, in particular into the stratosphere: A global data set for the past 100 years. Journal of Volcanology and Geothermal Research, 115(3-4), 511-528. https://doi.org/10.1016/S0377-
- Hammer, C. U. (1984). Traces of Icelandic eruptions in the Greenland ice sheet. Jökull Journal, 34(1), 51-65. https://doi.org/10.33799/ jokul11984.34.051
- Hammer, C. U., Clausen, H. B., & Dansgaard, W. (1980). Greenland ice sheet evidence of post-glacial volcanism and its climatic impact. Nature, 288(5788), 230-235. https://doi.org/10.1038/288230a0
- Hiles, W., Lawson, I. T., Roucoux, K. H., & Streeter, R. T. (2021). Late survival of woodland contrasts with rapid limnological changes following settlement at Kalmanstjörn, Mývatnssveit, northeast Iceland. Boreas, 50(4), 1209-1227. https://doi.org/10.1111/bor.12529
- Ilyinskaya, E., Schmidt, A., Mather, T. A., Pope, F. D., Witham, C., Baxter, P., et al. (2017). Understanding the environmental impacts of large fissure eruptions: Aerosol and gas emissions from the 2014-2015 Holuhraun eruption (Iceland). Earth and Planetary Science Letters, 472, 309-322. https://doi.org/10.1016/j.epsl.2017.05.025
- Jensen, B. J. L., Davies, L. J., Nolan, C., Pyne-O'Donnell, S., Monteath, A. J., Ponomareva, V., et al. (2021). A latest Pleistocene and Holocene composite tephrostratigraphic framework for northeastern North America. Quaternary Science Reviews, 272, 107242. https://doi.org/10.1016/ j.quascirev.2021.107242
- Jochum, K. P., Stoll, B., Herwig, K., Willbold, M., Hofmiann, A. W., Amini, M., et al. (2006). MPI-DING reference glasses for in situ microanalysis: New reference values for element concentrations and isotope ratios. Geochemistry, Geophysics, Geosystems, 7(2), Q02008. https://doi.org/10.1029/2005GC001060

HUTCHISON ET AL. 19 of 21

- Jongebloed, U. A., Schauer, A. J., Cole-Dai, J., Larrick, C. G., Wood, R., Fischer, T. P., et al. (2023). Underestimated passive volcanic sulfur degassing implies overestimated anthropogenic aerosol forcing. Geophysical Research Letters, 50(1), e2022GL102061. https://doi.org/10.1029/2022GL102061
- Krishnamohan, K. P. S. P., Bala, G., Cao, L., Duan, L., & Caldeira, K. (2019). Climate system response to stratospheric sulfate aerosols: Sensitivity to altitude of aerosol layer. Earth System Dynamics, 10(4), 885–900. https://doi.org/10.5194/esd-10-885-2019
- Kuehn, S. C., Froese, D. G., & Shane, P. A. R. (2011). The INTAV intercomparison of electron-beam microanalysis of glass by tephrochronology laboratories: Results and recommendations. *Quaternary International*, 246(1–2), 19–47. https://doi.org/10.1016/j.quaint.2011.08.022
- Larsen, G. (2000). Holocene eruptions within the Katla volcanic system, south Iceland: Characteristics and environmental impact. *Jökull Journal*, 49(49), 1–28. https://doi.org/10.33799/jokull2000.49.001
- Lawson, I., Gathorne-Hardy, F., Church, M., Newton, A., Edwards, K., Dugmore, A., & Einarsson, Á. (2007). Environmental impacts of the norse settlement: Palaeoenvironmental data from Mývatnssveit, northern Iceland. Boreas, 36(1), 1–19. https://doi.org/10.1080/03009480600827298
- Mackay, H., Hughes, P. D. M., Jensen, B. J. L., Langdon, P. G., Pyne-O'Donnell, S. D. F., Plunkett, G., et al. (2016). A mid to late Holocene cryptotephra framework from eastern North America. *Quaternary Science Reviews*, 132, 101–113. https://doi.org/10.1016/j.quascirev.2015.
- Mackay, H., Plunkett, G., Jensen, B. J. L., Aubry, T. J., Corona, C., Kim, W. M., et al. (2022). The 852/3 CE Mount Churchill eruption: Examining the potential climatic and societal impacts and the timing of the medieval climate anomaly in the north Atlantic region. *Climate of the Past*, 18(6), 1475–1508. https://doi.org/10.5194/cp-18-1475-2022
- Martin, E., Bekki, S., Ninin, C., & Bindeman, I. (2014). Volcanic sulfate aerosol formation in the troposphere. *Journal of Geophysical Research:* Atmospheres, 119(22), 12660–12673. https://doi.org/10.1002/2014JD021915
- Mason, E., Edmonds, M., & McConnell, J. R. (2022). Volatile trace metals deposited in ice as soluble volcanic aerosols during the 17.7 ka eruptions of Mt Takahe, West Antarctic Rift. Frontiers in Earth Science, 10(November), 1–11. https://doi.org/10.3389/feart.2022.1002366
- McCarthy, D., & Breen, A. (1997). An evaluation of astronomical observations in the Irish annals. Vistas in Astronomy, 41(1), 117–138. https://doi.org/10.1016/s0083-6656(96)00052-9
- McConnell, J. R., Burke, A., Dunbar, N. W., Köhler, P., Thomas, J. L., Arienzo, M. M., et al. (2017). Synchronous volcanic eruptions and abrupt climate change ~17.7 ka plausibly linked by stratospheric ozone depletion. *Proceedings of the National Academy of Sciences of the United States of America*, 114(38), 10035–10040. https://doi.org/10.1073/pnas.1705595114
- McConnell, J. R., Sigl, M., Plunkett, G., Burke, A., Kim, W. M., Raible, C. C., et al. (2020). Extreme climate after massive eruption of Alaska's Okmok volcano in 43 BCE and effects on the late Roman Republic and Ptolemaic Kingdom. Proceedings of the National Academy of Sciences of the United States of America, 117(27), 15443–15449. https://doi.org/10.1073/pnas.2002722117
- McConnell, J. R., Wilson, A. I., Stohl, A., Arienzo, M. M., Chellman, N. J., Eckhardt, S., et al. (2018). Lead pollution recorded in Greenland ice indicates European emissions tracked plagues, wars, and imperial expansion during antiquity. *Proceedings of the National Academy of Sciences* of the United States of America, 115(22), 5726–5731. https://doi.org/10.1073/pnas.1721818115
- Moreland, W. (2017). Explosive activity in flood lava eruptions: A case study of the 10th century Eldgjá eruption, Iceland. University of Iceland, School of Engineering and Natural Sciences, Faculty of Earth Sciences.
- Moreland, W. M., Thordarson, T., Houghton, B. F., & Larsen, G. (2019). Driving mechanisms of subaerial and subglacial explosive episodes during the 10th century Eldgjá fissure eruption, southern Iceland. Volcanica, 2(2), 129–150. https://doi.org/10.30909/vol.02.02.129150
- Morison, C. A. G., Oppenheimer, C., Thordarson, T., Newton, A. J., Moreland, W. M., & Dugmore, A. J. (2024). Disparate impacts of the Eldgjá and Laki flood-lava eruptions. *The Holocene*. https://doi.org/10.1177/09596836241254478
- Óladóttir, B. A., Larsen, G., & Sigmarsson, O. (2011). Holocene volcanic activity at Grímsvötn, Bárdarbunga and Kverkfjöll subglacial centres beneath Vatnajökull, Iceland. *Bulletin of Volcanology*, 73(9), 1187–1208. https://doi.org/10.1007/s00445-011-0461-4
- Óladóttir, B. A., Sigmarsson, O., Larsen, G., & Devidal, J. L. (2011). Provenance of basaltic tephra from Vatnajökull subglacial volcanoes, Iceland, as determined by major- and trace-element analyses. *The Holocene*, 21(7), 1037–1048. https://doi.org/10.1177/0959683611400456
- Oppenheimer, C., Orchard, A., Stoffel, M., Newfield, T. P., Guillet, S., Corona, C., et al. (2018). The Eldgiá eruption: Timing, long-range impacts and influence on the christianisation of Iceland. Climatic Change, 147(3–4), 369–381. https://doi.org/10.1007/s10584-018-2171-9
- Patris, N., Delmas, R. J., & Jouzel, J. (2000). Isotopic signatures of sulfur in shallow Antarctic ice cores. *Journal of Geophysical Research*, 105(D6), 7071–7078. https://doi.org/10.1029/1999JD900974
- Plunkett, G., & Pilcher, J. R. (2018). Defining the potential source region of volcanic ash in northwest Europe during the Mid-to Late Holocene. Earth-Science Reviews. 179(January), 20–37. https://doi.org/10.1016/j.earscirey.2018.02.006
- Plunkett, G., Sigl, M., McConnell, J. R., Pilcher, J. R., & Chellman, N. J. (2023). The significance of volcanic ash in Greenland ice cores during the Common Era. Quaternary Science Reviews, 301, 107936. https://doi.org/10.1016/j.quascirev.2022.107936
- Plunkett, G., Sigl, M., Pilcher, J. R., McConnell, J. R., Chellman, N., Steffensen, J. P., & Büntgen, U. (2020). Smoking guns and volcanic ash: The importance of sparse tephras in Greenland ice cores. *Polar Research*, 39(0), 1–11. https://doi.org/10.33265/polar.v39.3511
- Rhodes, R. H., Yang, X., & Wolff, E. W. (2018). Sea ice versus storms: What controls sea salt in arctic ice cores? *Geophysical Research Letters*, 45(11), 5572–5580. https://doi.org/10.1029/2018GL077403
- Sæmundsson, K., Jóhannesson, H., Hjartarson, Á., Kristinsson, S. G., & Sigurgeirsson, M. A. (2016). Geological map of Southwest Iceland, 1: 100000
- Savarino, J., Bekki, S., Cole-Dai, J., & Thiemens, M. H. (2003). Evidence from sulfate mass independent oxygen isotopic compositions of dramatic changes in atmospheric oxidation following massive volcanic eruptions. *Journal of Geophysical Research*, 108(21), 1–6. https://doi. org/10.1029/2003jd003737
- Schmid, M. M. E., Dugmore, A. J., Vésteinsson, O., & Newton, A. J. (2017). Tephra isochrons and chronologies of colonisation. *Quaternary Geochronology*, 40, 56–66. https://doi.org/10.1016/j.quageo.2016.08.002
- Schmidt, A., Thordarson, T., Oman, L. D., Robock, A., & Self, S. (2012). Climatic impact of the long-lasting 1783 Laki eruption: Inapplicability of mass-independent sulfur isotopic composition measurements. *Journal of Geophysical Research*, 117(23), D23116. https://doi.org/10.1029/2012JD018414
- Schneider, L., Smerdon, J. E., Büntgen, U., Wilson, R. J. S., Myglan, V. S., Kirdyanov, A. V., & Esper, J. (2015). Revising midlatitude summer temperatures back to A.D. 600 based on a wood density network. *Geophysical Research Letters*, 42(11), 4556–4562. https://doi.org/10.1002/2015GL063956
- Sieron, K., & Siebe, C. (2008). Revised stratigraphy and eruption rates of Ceboruco stratovolcano and surrounding monogenetic vents (Nayarit, Mexico) from historical documents and new radiocarbon dates. *Journal of Volcanology and Geothermal Research*, 176(2), 241–264. https://doi.org/10.1016/j.jvolgeores.2008.04.006
- Sigl, M., Winstrup, M., McConnell, J. R., Welten, K. C., Plunkett, G., Ludlow, F., et al. (2015). Timing and climate forcing of volcanic eruptions for the past 2,500 years. *Nature*, 523(7562), 543–549. https://doi.org/10.1038/nature14565

HUTCHISON ET AL. 20 of 21



### Journal of Geophysical Research: Atmospheres

- 10.1029/2023JD040142
- Sigurgeirsson, M. Á., Hauptfleisch, U., Newton, A., Einarsson, Á., Dxswàhlvfk, M. Á. S., & Einarsson, Á. (2013). Dating of the Viking age Landnám tephra sequence in lake Mývatn dating of the viking age Landnám tephra sequence in lake Mývatn. *Journal of the North Atlantic*, 21, 1–11
- Sinnl, G., Winstrup, M., Erhardt, T., Cook, E., Jensen, C. M., Svensson, A., et al. (2022). A multi-ice-core, annual-layer-counted Greenland ice-core chronology for the last 3800 years: GICC21. Climate of the Past, 18(5), 1125–1150. https://doi.org/10.5194/cp-18-1125-2022
- Stoffel, M., Khodri, M., Corona, C., Guillet, S., Poulain, V., Bekki, S., et al. (2015). Estimates of volcanic-induced cooling in the Northern Hemisphere over the past 1,500 years. *Nature Geoscience*, 8(10), 784–788. https://doi.org/10.1038/ngeo2526
- Stothers, R. B. (1998). Far reach of the Tenth century Eldgja eruption, Iceland. Climatic Change, 39(4), 715–726. https://doi.org/10.1023/A:1005323724072
- Sun, C., Plunkett, G., Liu, J., Zhao, H., Sigl, M., McConnell, J. R., et al. (2014). Ash from Changbaishan Millennium eruption recorded in Greenland ice: Implications for determining the eruption's timing and impact. Geophysical Research Letters, 41(2), 694–701. https://doi.org/ 10.1002/2013GL058642
- Textor, C., Graf, H. F., Herzog, M., & Oberhuber, J. M. (2003). Injection of gases into the stratosphere by explosive volcanic eruptions. *Journal of Geophysical Research*, 108(19), 1–17. https://doi.org/10.1029/2002jd002987
- Thordarson, T., & Larsen, G. (2007). Volcanism in Iceland in historical time: Volcano types, eruption styles and eruptive history. *Journal of Geodynamics*, 43(1), 118–152. https://doi.org/10.1016/j.jog.2006.09.005
- Thordarson, T., Miller, D. J., Larsen, G., Self, S., & Sigurdsson, H. (2001). New estimates of sulfur degassing and atmospheric mass-loading by the 934 AD Eldgjá eruption, Iceland. *Journal of Volcanology and Geothermal Research*, 108(1–4), 33–54. https://doi.org/10.1016/S0377-0273 (00)00277-8
- Thordarson, T., & Self, S. (1993). The Laki (Skaftár Fires) and Grímsvötn eruptions in 1783-1785. Bulletin of Volcanology, 55(4), 233–263. https://doi.org/10.1007/BF00624353
- Thordarson, T., & Self, S. (2003). Atmospheric and environmental effects of the 1783-1784 Laki eruption: A review and reassessment. *Journal of Geophysical Research*, 108(1), AAC7. https://doi.org/10.1029/2001jd002042
- van Dijk, E., Jungclaus, J., Lorenz, S., Timmreck, C., & Krüger, K. (2022). Was there a volcanic-induced long-lasting cooling over the Northern Hemisphere in the mid-6th-7th century? Climate of the Past, 18(7), 1601–1623. https://doi.org/10.5194/cp-18-1601-2022
- Watson, E. J., Swindles, G. T., Lawson, I. T., & Savov, I. P. (2016). Do peatlands or lakes provide the most comprehensive distal tephra records? Quaternary Science Reviews, 139, 110–128. https://doi.org/10.1016/j.quascirev.2016.03.011
- Watson, E. J., Swindles, G. T., Lawson, I. T., Savov, I. P., & Wastegård, S. (2017). The presence of Holocene cryptotephra in Wales and southern England. *Journal of Quaternary Science*, 32(4), 493–500. https://doi.org/10.1002/jqs.2942
- Wei, L., Mosley-Thompson, E., Gabrielli, P., Thompsn, L. G., & Barbante, C. (2008). Synchronous deposition of volcanic ash and sulfate aerosols over Greenland in 1783 from the Laki eruption (Iceland). Geophysical Research Letters, 35(16), 2–6. https://doi.org/10.1029/2008GL035117
- Wilson, R., Anchukaitis, K., Briffa, K. R., Büntgen, U., Cook, E., D'Arrigo, R., et al. (2016). Last millennium northern hemisphere summer temperatures from tree rings: Part I: The long term context. *Quaternary Science Reviews*, 134, 1–18. https://doi.org/10.1016/j.quascirev.2015.
- Witham, C. S., Aspinall, W. P., Braden, C., Hall, J., Loughlin, S. C., Schmidt, A., et al. (2015). UK hazards from a large Icelandic effusive eruption. In *Effusive eruption modelling project final report. Exeter, UK*. Retrieved from http://www.metoffice.gov.uk/research/news/2016/effusive-eruption-hazards%0Apapers3://publication/uuid/E08BFAC2-EEAD-4B4A-98A1-2B272068B91F
- Zambri, B., Robock, A., Mills, M. J., & Schmidt, A. (2019). Modeling the 1783–1784 Laki eruption in Iceland: 2. Climate impacts. *Journal of Geophysical Research: Atmospheres*, 124(13), 6770–6790. https://doi.org/10.1029/2018JD029554
- Zhong, Y., Miller, G. H., Otto-Bliesner, B. L., Holland, M. M., Bailey, D. A., Schneider, D. P., & Geirsdottir, A. (2011). Centennial-scale climate change from decadally-paced explosive volcanism: A coupled sea ice-ocean mechanism. *Climate Dynamics*, 37(11–12), 2373–2387. https://doi.org/10.1007/s00382-010-0967-z
- Zielinski, G. A., Germani, M. S., Larsen, G., Baillie, M. G. L., Whitlow, S., Twickler, M. S., & Taylor, K. (1995). Evidence of the Eldgjá (Iceland) eruption in the GISP2 Greenland ice core: Relationship to eruption processes and climatic conditions in the tenth century. *The Holocene*, 5(2), 129–140. https://doi.org/10.1177/095968369500500201

HUTCHISON ET AL. 21 of 21